PHYSICAL REVIEW D

PARTICLES AND FIELDS

THIRD SERIES, VOLUME 38, NUMBER 1 1 JULY 1988

Formation of spin-one mesons by photon-photon fusion

H. Aihara,[l] M. Alston-Garnjost,[a] R. E. Avery,[a] A. Barbaro-Galtieri,[a] A. R. Barker,[g] B. A. Barnett,[i] D. A. Bauer,[g] A. Bay,[a] H-U. Bengtsson,[d] G. J. Bobbink,[k] C. D. Buchanan,[d] A. Buijs,[k] D. O. Caldwell,[g] H-Y. Chao,[h] S-B. Chun,[d] A. R. Clark,[a] G. D. Cowan,[a] D. A. Crane,[i] O. I. Dahl,[a] M. Daoudi,[e] K. A. Derby,[a] J. J. Eastman,[a] P. H. Eberhard,[a] T. K. Edberg,[a] A. M. Eisner,[c] R. Enomoto,[l] F. C. Erné,[k] K. H. Fairfield,[f] J. M. Hauptman,[h] W. Hofmann,[a] J. Hylen,[i] T. Kamae,[l] H. S. Kaye,[a] R. W. Kenney,[a] S. Khacheryan,[d] R. R. Kofler,[j] W. G. J. Langeveld,[e] J. G. Layter,[e] W. T. Lin,[e] F. L. Linde,[k] S. C. Loken,[a] A. Lu,[g] G. R. Lynch,[a] R. J. Madaras,[a] B. D. Magnuson,[c] G. E. Masek,[f] L. G. Mathis,[a] J. A. J. Matthews,[i] S. J. Maxfield,[j] E. S. Miller,[f] W. Moses,[a] D. R. Nygren,[a] P. J. Oddone,[a] H. P. Paar,[f] S. K. Park,[h] D. E. Pellett,[b] M. Pripstein,[a] M. T. Ronan,[a] R. R. Ross,[a] F. R. Rouse,[a] K. A. Schwitkis,[g] J. C. Sens,[k] G. Shapiro,[a] B. C. Shen,[e] W. E. Slater,[d] J. R. Smith,[b] J. S. Steinman,[d] R. W. Stephens,[g] M. L. Stevenson,[a] D. H. Stork,[d] M. G. Strauss,[d] M. K. Sullivan,[c] T. Takahashi,[l] S. Toutounchi,[j] R. van Tyen,[a] G. J. VanDalen,[e] W. Vernon,[f] W. Wagner,[b] E. M. Wang,[a] Y-X. Wang,[g] W. A. Wenzel,[a] Z. R. Wolf,[a] H. Yamamoto,[a] S. J. Yellin,[g] and C. Zeitlin[b]

[a]*Lawrence Berkeley Laboratory, Berkeley, California 94720*

[b]*University of California, Davis, California 95616*

[c]*University of California Intercampus Institute for Research at Particle Accelerators, Stanford, California 94305*

[d]*University of California, Los Angeles, California 90024*

[e]*University of California, Riverside, California 92521*

[f]*University of California, San Diego, California 92093*

[g]*University of California, Santa Barbara, California 93106*

[h]*Ames Laboratory, Iowa State University, Ames, Iowa 50011*

[i]*Johns Hopkins University, Baltimore, Maryland 21218*

[j]*University of Massachusetts, Amherst, Massachusetts 01003*

[k]*National Institute for Nuclear and High Energy Physics, Amsterdam, The Netherlands*

[l]*University of Tokyo, Tokyo, Japan*

(TPC/Two-Gamma Collaboration)

(Received 9 February 1988)

We have observed the formation of two spin-one mesons in $\gamma\gamma$ fusion reactions in which one photon was highly virtual. The first, consistent with being the $J^{PC}=1^{++}$ $f_1(1285)$, was seen in the final state $\eta\pi^+\pi^-$ ($\eta\to\gamma\gamma$), as was the $\eta'(958)$. We have previously reported the observation of the second spin-one state, the $X(1420)$, in the final state $K^{\pm}K_S^0\pi^{\mp}$ ($K_S^0\to\pi^+\pi^-$). The formation of this state, which may be the $f_1(1420)$ observed in hadronic interactions, is reanalyzed using a new model and more data. We consider whether the $X(1420)$ could be the partner of the $f_1(1285)$ in the $J^{PC}=1^{++}$ meson nonet. The $\gamma\gamma^*$ width of each resonance was determined in several Q^2 bins. Using a model due to Cahn with a ρ form factor, we obtained for the coupling parameter $\tilde{\Gamma}_{\gamma\gamma}(f_1(1285))$ the value $2.4\pm0.5\pm0.5$ keV. We also found $B(X(1420)\to K\bar{K}\pi)\tilde{\Gamma}_{\gamma\gamma}(X(1420))=1.3\pm0.5\pm0.3$ keV using a ρ form factor, or $0.63\pm0.24\pm0.15$ keV using a ϕ form factor. The decay distributions of the observed $X(1420)$ events are consistent with a decay proceeding via $K^*(892)K$, and favor positive, but do not exclude negative, parity. Assuming that the $X(1420)$ and the $f_1(1285)$ are members of the same $q\bar{q}$ meson nonet and that $B(X(1420)\to K\bar{K}\pi)\approx 1$, and using a ϕ form factor in the model for $X(1420)$ formation, we determined the singlet-octet mixing angle of that nonet. The result, $(45.4\pm6.2)^\circ$, agrees well with the 42.2° implied by the Gell-Mann–Okubo quadratic mass formula; it is farther from the 35.3° ideal mixing angle. Our results are thus consistent with the $X(1420)$ being the mostly $s\bar{s}$ isoscalar member of the axial-vector $q\bar{q}$ meson nonet; however, we have no evidence contrary to hypotheses that the $X(1420)$ is an exotic $q^2\bar{q}^2$ or $q\bar{q}g$ state.

I. INTRODUCTION

The TPC/Two-Gamma Collaboration reported the first observation of the formation of a spin-one meson by $\gamma\gamma$ fusion in Ref. 1. Our observation of that state, whose mass is near 1420 MeV/c^2, was subsequently confirmed by the Mark II (Ref. 2) and JADE (Ref. 3) Collaborations. The Mark II Collaboration has also reported[4] observing the formation of a second spin-one state, with a mass near 1285 MeV/c^2. In each of these experiments, the reaction detected is

$$e^+e^- \rightarrow e^+e^-\gamma^*\gamma^* \rightarrow e^+e^-R \ , \tag{1}$$

where the resonance R is formed by the fusion of the two spacelike virtual photons (represented by the symbol γ^*). In this report, we present measurements of the formation of both the 1285- and 1420-MeV/c^2 spin-one states. We identify the first with the f_1 (1285), and consider whether the second, which we call the $X(1420)$, could be the other isoscalar member of the same meson nonet.

We begin the description of this analysis with a brief discussion of the general features of resonance formation by $\gamma\gamma$ fusion, and of those aspects peculiar to the spin-one case.

Each of the two virtual photons in reaction (1) is characterized by a value of Q^2, defined as the negative of its invariant mass squared (so that $Q^2>0$). If a photon has a sufficiently large Q^2, then the associated lepton will emerge from the reaction in a direction separated from that of the beam by an angle large enough to permit its detection; when detected, such final-state leptons are called *tags*. Photon-photon fusion reactions are operationally divided into three classes: untagged, in which both Q^2 values are small, singly tagged, and doubly tagged. In this paper we present analyses of untagged and singly tagged data. Since the effective flux of virtual photons per unit Q^2 is roughly proportional to $1/Q^2$, the effective $\gamma^*\gamma^*$ luminosity is reduced by a factor of 5–10 if it is required that a given lepton be tagged in a typical small-angle detector, and by the square of this factor if both leptons must be seen. The singly tagged statistics are doubled if electron-tag and positron-tag data are combined.

Because of the higher effective luminosity, and because tagged data can be collected only with a forward detector system, the formation of a resonance by $\gamma\gamma$ fusion has traditionally been observed first in untagged reactions. The cross section for this process is normally proportional to $\Gamma_{\gamma\gamma}(R)$, the partial width for the decay of the meson R to two photons. But if R has spin one, Yang's theorem[5,6] states that $\Gamma_{\gamma\gamma}(R)$ must vanish. Spin-one mesons can be produced by $\gamma\gamma$ fusion, but QED and dimensional analysis together imply that the cross section will be very small compared to that for the formation of spin-zero or spin-two mesons until the Q^2 of at least one of the virtual photons becomes comparable to a characteristic mass squared. While this mass squared is in principle unknown, it is probably on the order of the invariant mass squared of the resonance or at least the ρ-meson mass squared. A peak seen in an invariant-mass spectrum of tagged data, when there is no peak in the corresponding spectrum of untagged data, is therefore characteristic of the formation of spin-one mesons.

Measurements of $\Gamma_{\gamma\gamma}(R)$ based on $\gamma\gamma$ fusion data have been used to study the quark content of the pseudoscalar resonances π^0, η, and $\eta'(958)$, as well as the tensor states $a_2^0(1320)$, $f_2(1270)$, and $f_2'(1525)$ (Refs. 7–10). As more tagged data are collected, it may become possible to use measurements of the cross sections for the formation of spin-one mesons to study the less-well-understood nonet of axial-vector mesons, in which the valence $q\bar{q}$ pair is in a $^3P_1$ state. That nonet must include two isoscalar states: one of these is the $f_1(1285)$; the other, not yet firmly identified, we refer to here as the f_1'. Since the $f_1(1285)$ is much more likely to decay to $\pi\pi\pi\pi$ than to $K\bar{K}\pi$ (Ref. 11) and has a mass near that of the $a_1(1270)$, it is usually assumed to be composed mostly of u and d quarks. This would imply that the SU(3)-singlet and -octet components of the axial-vector-meson nonet are nearly ideally mixed, so that the f_1' is a mostly $s\bar{s}$ state. On the other hand, the recent observation of the decay $f_1(1285)\rightarrow\gamma\phi(1020)$ (Ref. 12) and the relatively high branching fraction for the decay $J/\psi\rightarrow\phi(1020)f_1(1285)$ compared to that for $J/\psi\rightarrow\omega(783)f_1(1285)$ (Refs. 13 and 14) may imply a significant deviation from ideal mixing.

The f_1' has sometimes been identified[11] with the $f_1(1420)$, a state observed in hadronic interactions.[15,16] Its mass and the fact that its only known decay is to the final state $K\bar{K}\pi$ support this identification, but uncertainties remain: for example, the LASS Collaboration found no clear evidence for the peripheral hypercharge-exchange reaction $K^-p\rightarrow f_1(1420)\Lambda$ (Ref. 17), which they state would be expected to occur if the $f_1(1420)$ were the f_1'. Also, the Mark III Collaboration has reported[13] observing a state $X_{\rm Mk3}$ in the decay $J/\psi\rightarrow\omega(783)X_{\rm Mk3}$, and not in the related process $J/\psi\rightarrow\phi(1020)X_{\rm Mk3}$; the spin of the $X_{\rm Mk3}$ is unknown, but its mass and width are consistent with those of the $f_1(1420)$ and not with those of $\eta(1440)$ (Ref. 18). We note, however, that the interpretation of results concerning J/ψ hadronic decays to final states consisting of $\omega(783)$ or $\phi(1020)$ and an f_1 meson is complicated by a recent theoretical study[19] which concludes that the contribution of doubly-Okubo-Zweig-Iizuka-rule-violating J/ψ decay diagrams may be more important than has generally been supposed.

The LASS Collaboration did observe the production of a higher-mass $J^{PC}=1^{++}$ state, the $f_1(1530)$, in the reaction $K^-p\rightarrow f_1(1530)\Lambda$ (Ref. 17). Their data confirm the existence of this state, which was first observed by Gavillet *et al.*,[20] and was originally called the $D'(1530)$. Like the $f_1(1420)$, the $f_1(1530)$ decays to $K\bar{K}\pi$; it too has been proposed as the f_1'. But if the $f_1(1530)$ were the f_1', the composition of the $f_1(1420)$ would remain to be understood. There has been considerable speculation concerning the question of what the $f_1(1420)$ might be, if it is not the f_1'; recent suggestions include a $q^2\bar{q}^2$ state[21] and a $q\bar{q}g$ hybrid with the exotic quantum numbers $J^{PC}=1^{-+}$ (Ref. 22).

Since the $\gamma\gamma$-$q\bar{q}$ coupling is proportional to the square

of the quark charge, the cross section for the formation of a pure $s\bar{s}$ meson by $\gamma\gamma$ fusion is expected to be small compared to that for a meson with a large $u\bar{u}$ content. The cross section for formation of the $X(1420)$ we reported in Ref. 1 was considerably greater than that predicted for a pure $s\bar{s}$ f_1' at that mass. This may indicate the presence of significant u and d quark content in the f_1', or that the $X(1420)$ is a state distinct from the f_1'. The predictions of small cross sections, however, are highly model dependent and are based on inherently uncertain comparisons with other meson nonets. Some of these uncertainties can be removed only by measuring the cross sections for formation of the other known nonstrange $J^{PC}=1^{++}$ mesons, the $f_1(1285)$ and $a_1^0(1270)$. The very large width of the $a_1^0(1270)$ (Refs. 11 and 23) makes it difficult to observe; the difficulty is aggravated by the limited statistics (largely a consequence of the relativity low integrated $\gamma^*\gamma^*$ luminosities currently available) and by the proximity of the $a_2^0(1320)$. We have therefore concentrated on observing the $f_1(1285)$. In this paper we describe our observation of that state, and compare its formation by $\gamma\gamma$ fusion with that of the $X(1420)$.

This paper continues in Sec. II with a summary of the general formalism used to describe the formation of resonances by $\gamma\gamma$ fusion. This is followed in Sec. III by a description of our experiment. In Sec. IV we present an analysis of the $\eta\pi^+\pi^-$ ($\eta\to\gamma\gamma$) final state, one of the principal decay modes of the $f_1(1285)$. Section V presents results, obtained from our analysis of the $\eta\pi^+\pi^-$ channel, concerning the formation of the $\eta'(958)$. These results are then compared with those of other experiments, as a check of our Monte Carlo acceptance calculation for that final state. Section VI describes a model due to Cahn[24] for the formation of axial-vector $q\bar{q}$ bound states, and discusses its application to our $f_1(1285)$ signal. In Sec. VII, we briefly describe our analysis of the $\pi^+\pi^-\pi^+\pi^-$ final state, another important decay mode of the $f_1(1285)$.

Section VIII contains a description of our analysis of the $K^{\pm}K_S^0\pi^{\mp}$ ($K_S^0\to\pi^+\pi^-$) final state. In Sec. IX we present new results from that analysis. These principally concern the $X(1420)$, and include a discussion of our investigation into its parity. In Sec. X we compare our $f_1(1285)$ and $X(1420)$ results: specifically, we assume that the $X(1420)$ is the f_1' and that it decays only to $K\bar{K}\pi$, and determine the singlet-octet mixing angle for the $J^{PC}=1^{++}$ meson nonet to which our results would then correspond. We conclude in Sec. XI with a summary of our findings.

II. GENERAL FORMALISM FOR PHOTON-PHOTON FUSION

To lowest order in QED, the differential cross section for the reaction $e^+e^-\to e^+e^-S$, where the final state S is produced by $\gamma\gamma$ fusion, may be expressed in terms of the cross sections for $\gamma^*\gamma^*\to S$ according to the relation[25]

$$\frac{E_1E_2d^6\sigma}{d^3\mathbf{p}_1d^3\mathbf{p}_2}=\sum_{i,j}\mathcal{L}_{ij}\sigma_{ij}\ . \tag{2}$$

Here i and j can each be either L (longitudinal photon polarization) or T (transverse photon polarization) and the $\mathcal{L}_{ij}$ are calculable virtual-photon flux factors. E_1, E_2, $\mathbf{p}_1$, and $\mathbf{p}_2$ are the energies and momenta of the outgoing positron and electron , respectively. Interference terms that integrate to zero over $\tilde{\phi}$, where $\tilde{\phi}$ is the separation in azimuthal angle of the final-state lepton momenta in the $\gamma^*\gamma^*$ center of mass, have been omitted.

We define virtual $\gamma\gamma$ widths $\Gamma^{ij}_{\gamma^*\gamma^*}$ for a resonance of mass M, spin J, and total width Γ, by

$$\sigma_{ij}=\frac{32\pi(2J+1)}{N_iN_j}\frac{W^2}{2\sqrt{X}}\left[\frac{\Gamma}{(W^2-M^2)^2+\Gamma^2M^2}\right]\times\Gamma^{ij}_{\gamma^*\gamma^*}(Q_1^2,Q_2^2,W^2)\ . \tag{3}$$

In this equation, $N_L=1$ and $N_T=2$; $W=[(q_1+q_2)^2]^{1/2}$, and $X=(q_1\cdot q_2)^2-q_1^2q_2^2$, where the q_i are the virtual-photon four-momenta. The N_i are the number of virtual-photon polarization states, W is the invariant mass of the final state S, and the Møller flux factor $\sqrt{X}$ is equal to kW, where k is the magnitude of the virtual-photon momenta in the $\gamma^*\gamma^*$ center of mass.[26]

In a singly tagged event, only one of the two Q^2 values is measured; the other is generally much smaller. It is therefore convenient to define $\gamma\gamma^*$ widths by taking the limit in which the invariant mass squared ($-P^2$) of the virtual photon emitted by the unobserved final-state lepton approaches zero:

$$\Gamma^{ij}_{\gamma\gamma^*}(Q^2,W^2)\equiv\begin{cases}\lim\limits_{P^2\to0}\Gamma^{ij}_{\gamma^*\gamma^*}(Q^2,P^2,W^2) & \text{if the } e^+ \text{ is tagged ,}\\ \lim\limits_{P^2\to0}\Gamma^{ji}_{\gamma^*\gamma^*}(P^2,Q^2,W^2) & \text{if the } e^- \text{ is tagged .}\end{cases} \tag{4}$$

In the experiment described here, the average value of P^2 was approximately 0.004 GeV^2. This value is much smaller than the W^2 values possible for the final states discussed in this paper; it is also smaller than the measured Q^2 values, which were greater than 0.1 GeV^2. The difference between the limits appearing in Eq. (4) and the functions derived from our singly tagged data should therefore be negligible.

Gauge invariance requires that any width involving a longitudinally polarized virtual photon whose invariant mass squared is $-Q^2$ be proportional to Q^2 as Q^2 approaches zero. Hence only $\Gamma^{LT}_{\gamma\gamma^*}$ and $\Gamma^{TT}_{\gamma\gamma^*}$ are nonzero,

and $\Gamma^{LT}_{\gamma\gamma^*}(Q^2,W^2)$ must itself vanish as Q^2 approaches zero. Our definitions also imply that, for any resonance R,

$$\lim_{Q^2\to 0}\Gamma^{TT}_{\gamma\gamma^*}(Q^2,M_R^2)=\Gamma_{\gamma\gamma}(R)\ , \tag{5}$$

where $\Gamma_{\gamma\gamma}(R)$ is the partial width for the decay of R to two real photons.

A spin-zero resonance can be formed by $\gamma\gamma$ fusion only when the interacting virtual photons have equal helicities; in order to form a pseudoscalar resonance, the photons must also be transversely polarized. If P is a pseudoscalar resonance with $\Gamma_{\gamma\gamma}(P)\neq 0$, such as the $\eta'(958)$ discussed in Sec. V, we define its $\gamma\gamma^*$ form factor, $F(Q^2,W^2)$, by the relation[27]

$$\Gamma^{TT}_{\gamma\gamma^*}(Q^2,W^2)=\frac{4X}{W^4}F^2(Q^2,W^2)\Gamma_{\gamma\gamma}(P)\ . \tag{6}$$

The form factor satisfies the normalization condition $F^2(0,M_P^2)=1$. In practice, $\Gamma_{\gamma\gamma}(P)$ is usually determined from the cross section for the formation of P in untagged $\gamma\gamma$ fusion reactions; tagged data are then used to extract $F^2(Q^2,M_P^2)$ in the Q^2 range accessible to the experiment. When the meson P is relatively narrow, as is the $\eta'(958)$, we generally set $W=M_P$ and refer to $\Gamma^{TT}_{\gamma\gamma^*}(Q^2)$ and $F(Q^2)$, omitting the second argument.

Whereas in the spin-zero case $\Gamma^{LT}_{\gamma\gamma^*}(Q^2,W^2)$ is identically zero, both $\Gamma^{TT}_{\gamma\gamma^*}$ and $\Gamma^{LT}_{\gamma\gamma^*}$ may contribute to the cross section for the formation of a spin-one resonance. When $J=1$, interactions described by $\Gamma^{TT}_{\gamma\gamma^*}(Q^2,W^2)$ involve virtual photons with equal helicities. But for any resonance R with odd spin, Bose symmetry requires that the matrix element for the reaction $\gamma^*\gamma^*\to R$ vanish when the two virtual photons are identical: i.e., when their helicities are the same and their Q^2 values are equal. Since the square of the matrix element must be an analytic function of Q_1^2 and Q_2^2, symmetric under their interchange, $\Gamma^{TT}_{\gamma^*\gamma^*}(Q_1^2,Q_2^2,W^2)$ for a spin-one resonance must be proportional to $(Q_1^2-Q_2^2)^2$ whence $\Gamma^{TT}_{\gamma\gamma^*}(Q^2,W^2)\propto(Q^2)^2$ as Q^2 approaches zero. Together with Eq. (5), this implies Yang's theorem: $\Gamma_{\gamma\gamma}(A)=0$ for any spin-one resonance A (Refs. 5 and 6).

Because of Yang's theorem, the separation of normalization and Q^2 dependence for spin-one-meson formation differs from that used in the pseudoscalar case. If A is a spin-one resonance, we define the $\gamma\gamma$-A coupling parameter $\tilde{\Gamma}_{\gamma\gamma}(A)$ by

$$\tilde{\Gamma}_{\gamma\gamma}(A)\equiv\lim_{Q^2\to 0}\frac{M_A^2}{Q^2}\Gamma^{LT}_{\gamma\gamma^*}(Q^2,M_A^2)\ . \tag{7}$$

$\tilde{\Gamma}_{\gamma\gamma}(A)$ is difficult to determine using only this definition, since that would require measurements of the formation of the meson A at low Q^2, where the cross section is expected to be very small, and where tagging is difficult. If a specific model for the Q^2 evolution of both $\Gamma^{LT}_{\gamma\gamma^*}$ and $\Gamma^{TT}_{\gamma\gamma^*}$ is used, then $\tilde{\Gamma}_{\gamma\gamma}(A)$ can be determined from data at higher Q^2, if that model is correct. In Sec. VI we discuss one such model, due to Cahn,[24] for the reaction $\gamma^*\gamma^*\to A$. It should be noted that Cahn's convention for the definition of $\Gamma^{ij}_{\gamma^*\gamma^*}$ in the $J=1$ case, which is used by the Mark II Collaboration in Refs. 2 and 4, results in $\tilde{\Gamma}_{\gamma\gamma}(A)$ values twice as large as ours.[28] A recent paper by Olsson includes a brief discussion of the differences between the two conventions.[29]

$\Gamma^{LT}_{\gamma\gamma^*}$ and $\Gamma^{TT}_{\gamma\gamma^*}$ can in principle be measured separately by exploiting the differing angular distributions resulting from the decays of transversely and longitudinally polarized spin-one mesons, but such a separation cannot be made with low-statistics data. Given this limitation, we are sensitive only to the total cross section, which depends on the combination

$$\Gamma_{\gamma\gamma^*}(Q^2,W^2)\equiv[1+\epsilon^{-1}\mathcal{R}(Q^2,W^2)]\Gamma^{LT}_{\gamma\gamma^*}(Q^2,W^2)\ , \tag{8}$$

In this equation, ϵ^{-1} represents the average value of $\mathcal{L}_{TT}/\mathcal{L}_{LT}$ (Ref. 30) over the phase space for singly tagged $\gamma\gamma$ fusion events with the given Q^2 and W^2, and the function $\mathcal{R}$ is defined by

$$\mathcal{R}(Q^2,W^2)\equiv\frac{\sigma_{TT}}{\sigma_{LT}}\ . \tag{9}$$

The value of ϵ depends on the kinematic region in which tags are detected; in our experiment, $\epsilon\approx 1$. If $\tilde{\Gamma}_{\gamma\gamma}(A)\neq 0$, then $\mathcal{R}(Q^2,W^2)$ must vanish as Q^2 approaches zero. If A is an axial-vector meson satisfying this condition, we define its effective $\gamma\gamma^*$ form factor, $\tilde{F}(Q^2,W^2)$, by the relation

$$\Gamma_{\gamma\gamma^*}(Q^2,W^2)=\frac{4X}{W^4}\tilde{F}^2(Q^2,W^2)\tilde{\Gamma}_{\gamma\gamma}(A)\ . \tag{10}$$

Defined thus, $\tilde{F}$ will satisfy the two conditions:

$$\lim_{Q^2\to 0}\tilde{F}^2(Q^2,W^2)=0\ , \tag{11a}$$

$$\lim_{Q^2\to 0}\frac{M_A^2}{Q^2}\tilde{F}^2(Q^2,M_A^2)=1\ . \tag{11b}$$

As in the pseudoscalar case, if the meson A is relatively narrow, we usually put $W=M_A$ and omit the second argument in these functions.

III. THE EXPERIMENT

The data described in this paper were collected with the TPC/Two-Gamma detector facility[31] at SLAC. The observed $\gamma\gamma$ fusion events resulted from interactions of 14.5-GeV electrons and positrons in the PEP storage ring.

In the analysis of these data, the Time Projection Chamber (TPC) was used in conjunction with a solenoidal magnetic field to detect charged particles produced at angles more than 340 mrad from the beam direction and to measure their momenta. Initially the field strength was 0.389 T, providing momentum resolution of approximately 6% at large angles for the relatively low momenta involved in $\gamma\gamma$ fusion reactions. Following the installation of a superconducting magnet coil, the field strength was increased to 1.325 T. Other improve-

ments made to the TPC included an improved calibration procedure, a 25% reduction in the material between the interaction point and the inner radius of the TPC, and a gated grid system that reduced space-charge distortions. The net effect of the combination of these changes and the stronger magnetic field was to improve the TPC momentum resolution for low momenta to about 1.5%.

The TPC was also used to identify charged particles by measuring each track's rate of ionization energy loss. This was accomplished by comparing the dE/dx value (defined as the average of the lowest 65% of up to 183 measurements along the track) to that expected for each stable particle species, given the measured momentum. The resulting likelihoods for the various identification hypotheses were expressed as a set of χ^2 values $(\chi_e^2,\chi_\mu^2,\chi_\pi^2,\chi_K^2,\chi_p^2)$ (Refs. 32 and 31). An inspection of the distribution of dE/dx measurements about the expected values, using tracks left by particles whose identity was known by other means, indicated a dE/dx resolution of approximately 3.5%.

Additional charged-particle tracking was provided by a series of 15 planes of drift chambers in the forward regions, between 25 and 180 mrad from the beam direction. A septum magnet with $\int \mathbf{B}\cdot d\mathbf{l}=0.26$ T m allowed the measurement of charged particle momenta using these chambers. Cherenkov counters and muon chambers covering these regions assisted in particle identification. The muon and pion thresholds in the Cherenkov counters were 3.5 and 4.5 GeV/c, respectively.

Tags were detected, and their energies measured, using calorimeters in both forward regions. Two arrays of 60 NaI crystals had fiducial volumes that covered the region between 25 and 90 mrad from the beam direction. From 100 to 180 mrad, lead/scintillator shower counters (SHW) were used. Tags were identified by the presence of a high-energy shower in one of these calorimeters, in conjunction with matching hits in the forward drift chambers. The excellent energy resolution of the NaI arrays ($\sigma_E/E\approx 1.2\%$ for elastically scattered 14.5-GeV electrons) enabled us to determine the Q^2 of the corresponding virtual photon with a relative uncertainty that was usually less than 3%. At larger angles, the uncertainty in Q^2 was greater, due to the poorer energy resolution of the shower counters ($\sigma_E/E\approx 5.5\%$ at 14.5 GeV). The angular coverage of the NaI and SHW detectors allowed us to observe tags corresponding to virtual photons with Q^2 values between roughly 0.05 and 7 GeV^2. To ensure good tagging efficiency, the analyses described here used only the Q^2 region between 0.1 and 5 GeV^2.

Photon momenta were measured using various calorimeters. Their properties have been described elsewhere,[31] so we specify here only the type of each calorimeter, and the region covered by its fiducial volume. In the forward regions, between 25 and 180 mrad from the beam, the NaI and SHW calorimeters described above were also used for photon detection. Although the energy resolution of these calorimeters was measured only with Bhabha events, we assumed $\sigma_E/E\propto E^{-1/4}$ for the NaI, and $\sigma_E/E\propto E^{-1/2}$ for the shower counters. In all resolution formulas, E is the deposited energy in GeV.

Between 300 and 600 mrad from the beam, proportional-mode pole-tip calorimeters (PTC) measured shower energies with a σ_E/E approximately $16\%/\sqrt{E}$ for $E<1$ GeV. In the barrel region, a Geiger-mode hexagonal calorimeter (HEX) was located outside the magnet coil, covering angles more than 700 mrad from the beam. Photon energy resolution in the HEX was estimated at $\sigma_E/E\approx 17\%/E^{1/4}$ for $E<1$ GeV, and was somewhat worse if the photon converted in the coil, rather than in the HEX itself. A cylindrical outer drift chamber (ODC) between the coil and the HEX was used to identify such early conversions; when ODC hits were matched to a HEX photon, an energy-dependent correction was added to the shower energy measured in the HEX to compensate for losses in the coil.

In addition to isolated showers in the various calorimeters, we allowed reconstructed e^+e^- conversion pairs in the TPC as final-state photons. Both tracks in these pairs were required to have measured dE/dx values and momenta such that $\chi_e^2<8$. The invariant mass of each pair was required to be less than 50 MeV/c^2. Although conversions sometimes take place in the TPC volume, they generally occur in the material between the vertex and the TPC inner radius, which amounted to about 0.18 radiation lengths before 1984 (low-field data), and 0.14 radiation lengths thereafter (high-field data). To avoid misidentifying e^+e^- pairs produced at the interaction point as conversion pairs, we required that the point of closest approach of the two tracks be at least 5 cm from the beam.

As discussed in Sec. I, the data are separated into two subsets: the tagged data, in which either the electron or positron was observed in the forward detectors, and the untagged data, in which neither lepton was seen. The untagged data described here correspond to an integrated luminosity estimated at 140 pb^{-1}, of which 65 pb^{-1} were recorded after installation of the superconducting magnet coil. The integrated luminosity of the tagged data is estimated at 114 pb^{-1}, including 63 pb^{-1} with the superconducting coil. The tagged-data values are lower than those for the untagged data primarily because high levels of small-angle background sometimes prevented operation of the forward detector systems.

Untagged events were required to have satisfied at least one of two triggers. The first of these required two tracks in different 60° azimuthal sectors of the TPC. For triggering purposes, such tracks had to have momenta whose directions were separated from the beam by at least 450 mrad in the high-field data and by at least 560 mrad in the low-field data. In addition, hits were required in the inner drift chamber (IDC), a cylindrical drift chamber between the beam pipe and the TPC. Any track more than 780 mrad from the beam was required to coincide in azimuth with hits in the ODC as well. Pions produced in this region with transverse momenta less than about 200 MeV/c were stopped by ionization energy losses in the coil; such pions consequently failed to produce the required ODC hits. The other untagged trigger required one track in the TPC in coincidence with energy deposited in the PTC or HEX. In order to set this trigger, the total measured energy had to exceed thresholds set between 0.7 and 1.3 GeV in the HEX, and be-

tween 2 and 4 GeV in the PTC.

Three tagged triggers were used, each of which required the presence of energy consistent with a tag in either the NaI or SHW calorimeters. The first of these required coincident energy deposition in the PTC or HEX above thresholds ranging from 0.3 to 1.0 GeV. The second tagged trigger, used only in the analysis of the low-field data, required coincident IDC hits. During the latter part of the acquisition of the low-field data, the definition of this trigger was modified to allow tag-candidate showers in the NaI at angles closer to the beam than had previously been allowed, provided the shower coincided with hits in both the ODC and IDC. The third tagged trigger, used primarily in the analysis of the high-field data, required IDC hits in coincidence with a single TPC track, which had to satisfy the same criteria as did TPC tracks contributing to the untagged triggers.

IV. ANALYSIS OF THE $\eta\pi^+\pi^-$ FINAL STATE

The $f_1(1285)$ decays via three channels: $\eta\pi\pi$, with a branching fraction B of $(49\pm7)\%$, $\pi\pi\pi\pi$, with $B=(40\pm7)\%$, and $K\bar{K}\pi$, with $B=(11\pm3)\%$ (Ref. 11). We first describe our observation of the $f_1(1285)$ in the $\eta\pi\pi$ channel. In particular, we consider the final state $\eta\pi^+\pi^-$, with the subsequent decay $\eta\to\gamma\gamma$. Since $\frac{1}{3}$ of the $\eta\pi\pi$ decays of the $f_1(1285)$ are to $\eta\pi^0\pi^0$, and 61% of η decays are to final states other than $\gamma\gamma$, the net branching fraction for the decay chain leading to the final state $\pi^+\pi^-\gamma\gamma$ is $(12.7\pm1.8)\%$.

To search for the $f_1(1285)$ in this final state, we selected both tagged and untagged events containing exactly two oppositely charged tracks in the TPC, each with $\chi^2_\pi<10$. In addition, we selected tagged events having exactly one TPC track with $\chi^2_\pi<10$ and one oppositely charged track in the forward drift chambers. The forward track in these events had to have no matching hits in the forward Cherenkov counters or muon chambers, and the magnitude of its measured momentum had to be between 0.3 and 3.5 GeV/c. TPC tracks originating far from the interaction point, or belonging to reconstructed conversion pairs, were not counted for the purpose of either of these selection criteria.

Since the curves describing the dE/dx expected of each particle species as a function of momentum cross each other, the measured momentum and dE/dx sometimes fail to identify a track unambiguously. To reduce background arising from events in which such ambiguous tracks are misidentified as pions, we required $\sum\chi^2_\pi+4<\min(\sum\chi^2_e,\sum\chi^2_K,\sum\chi^2_p)$, where the sums are over the pion-candidate TPC tracks. We also demanded that these tracks satisfy vertex cuts, be no less than 420 mrad from the beam direction, and have estimated momenta at the interaction point whose magnitudes were greater than 120–210 MeV/c, depending on the direction of the track and the magnetic field strength. The relative uncertainty in the measurement of the magnitude of each track's momentum was required to be less than 30%.

Each event was also required to contain two photons. A photon was defined in one of two ways: it could be a reconstructed conversion pair satisfying the requirements stated in Sec. III, or it could be a shower in any of the calorimeters which (1) was located in the fiducial volume of the calorimeter, (2) contained energy exceeding minima between 50 and 500 MeV, depending on the calorimeter, and (3) was not too near the extrapolated position of any charged track in the event.

Tags were required to deposit at least 4 GeV in a NaI array, or 8 GeV in one of the shower counters. They also had to satisfy fiducial cuts designed to ensure accurate measurement of Q^2. Doubly tagged events were rejected.

The cross section for formation of $\pi^+\pi^-$ and $\mu^+\mu^-$ pairs by $\gamma\gamma$ fusion is relatively large.[33] To reject background due to such events, where the showers identified as photons coming from the event vertex were actually secondary interaction products, or were otherwise not produced in the $\gamma\gamma$ fusion reaction, we demanded in the untagged case that the azimuthal separation of the pion tracks be less than 170°; in the tagged case we demanded instead that the magnitude of the total transverse momentum of the tag and the two pions be greater than 80 MeV/c. Background from e^+e^- annihilation reactions was rejected by a requirement that the sum of the magnitudes of the pion and photon momenta be less than 10 GeV/c. Finally, to reduce nonexclusive backgrounds, the total transverse momentum of each event, including the photons (and the tag, if any), was required to have a magnitude less than 300 MeV/c.

These cuts left a total of 2813 untagged, and 1090 tagged, exclusive $\pi^+\pi^-\gamma\gamma$ candidate events. In addition to the remaining nonexclusive background, these samples contain events due to the formation of the exclusive final state $\pi^+\pi^-\pi^0$. The relatively poor photon energy resolution makes it difficult to separate these contributions reliably on the basis of $\gamma\gamma$ invariant masses calculated using the measured photon energies. To facilitate the separation, we subjected each event to a constrained kinematic fit, in which the total transverse momentum of the observed particles in the event was required to be zero, with a 20-MeV/c uncertainty. Many of the remaining nonexclusive events should fail this two-constraint (2C) fit. Furthermore, the fitted $\gamma\gamma$ invariant mass for exclusive events is generally closer to the true value than is the unfitted mass. Since $\eta\pi^+\pi^-$ events are characterized by relatively high photon energies, we also required that both fitted photon energies be greater than 125 MeV (Ref. 34). Figure 1 shows the resulting fitted $\gamma\gamma$ mass spectra for untagged and tagged events passing the 2C fit with a confidence level greater than 2%. Clear π^0 and η peaks are seen in both spectra.

Next, $\eta\pi^+\pi^-$ candidates were selected from the set of events passing the 2C fit by the requirement that their fitted $\gamma\gamma$ mass be within 150 MeV/c^2 of M_η. This cut was chosen on the basis of the expected $\gamma\gamma$ mass resolution. These events were refit, with the additional constraint $M_{\gamma\gamma}=M_\eta$. Events were rejected if they failed to pass this 3C fit with a confidence level of at least 3%, or if either photon energy resulting from the fit fell below 125 MeV (Ref. 34). All events passing the second fit were scanned by eye in order to remove those that were not properly reconstructed. Such events might have had very

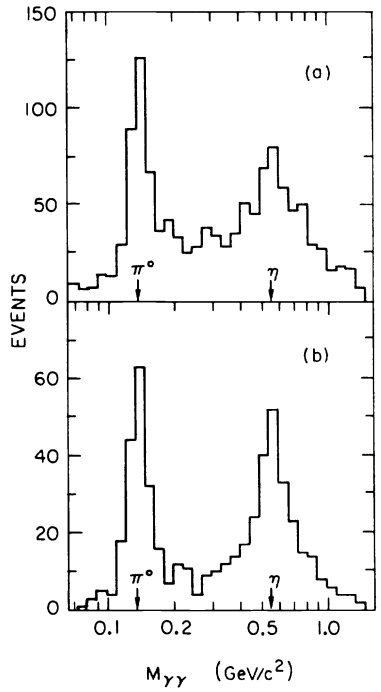

FIG. 1. The two-constraint fitted $\gamma\gamma$ invariant-mass spectra for $\pi^+\pi^-\gamma\gamma$ events: (a) untagged data and (b) tagged data.

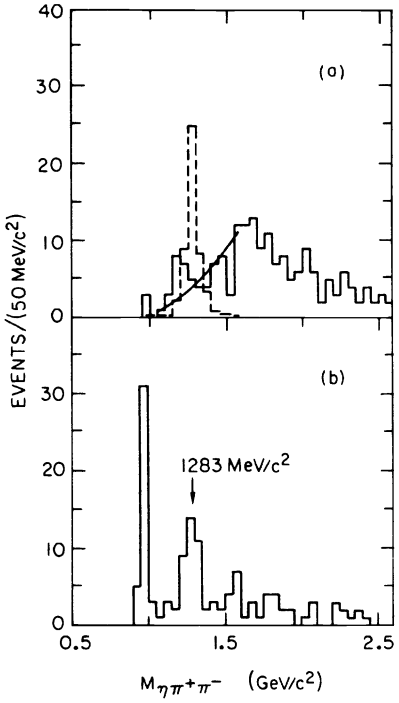

FIG. 2. The three-constraint-fitted $\eta\pi^+\pi^-$ invariant-mass spectra of the final event samples: (a) untagged data and (b) tagged data. The dashed histogram in (a) shows the peak expected at 1285 MeV/c^2 if the peak in (b) were due to formation of a resonance with $J\neq 1$. The curve in (a) represents the background estimate used to derive the upper limit given in Sec. VI.

low angle TPC tracks, or "photons" that were actually showers produced by nonvertex tracks, backscattered tracks, or nuclear interaction products. We rejected about 20% of the events scanned for these or similar reasons.

The final samples consist of 197 untagged and 129 tagged events. The 3C-fitted $\eta\pi^+\pi^-$ invariant-mass spectra are shown in Fig. 2. The spectrum of tagged data includes two clear peaks: the lower-mass peak is due to formation of the $\eta'(958)$; in Sec. VI we will ascribe the second peak to formation of the $f_1(1285)$. There are, on the other hand, no obvious peaks in the spectrum of untagged data. The pseudoscalar $\eta'(958)$ is known to be formed in untagged $\gamma\gamma$ fusion reactions; the absence of an $\eta'(958)$ signal in our untagged $\eta\pi^+\pi^-$ data must therefore be a consequence of low experimental acceptance. We will describe in the next section why our untagged $\eta\pi^+\pi^-$ acceptance at $W=M_{\eta'}$ is low enough to account for the paucity of untagged $\eta'(958)\to\eta\pi^+\pi^-$ ($\eta\to\gamma\gamma$) events. We will also show that low acceptance cannot be used to explain the absence of the higher-mass peak in the untagged invariant-mass spectrum; that peak must be due to the formation of a spin-one state.

V. $\eta'(958)$ RESULTS

The formation of the $\eta'(958)$ by $\gamma\gamma$ fusion has been observed by a number of experiments in both tagged and untagged data.[35–42,4] We can therefore use the $\eta'(958)$ signal in our tagged $\eta\pi^+\pi^-$ data, as well as the near absence of a signal in the corresponding untagged data, to check our Monte Carlo acceptance calculation for the $\eta\pi^+\pi^-$ final state.

To determine $\Gamma^{TT}_{\gamma\gamma *}(Q^2)$ for the $\eta'(958)$, we used the formulas presented in Sec. II to simulate both untagged and tagged $\eta'(958)$ formation. The Monte Carlo simulation included the effects of nuclear and electromagnetic interactions with the materials in the detectors, as well as inefficiencies due to detector response, triggering, and the event selection and fitting procedure described in Sec. IV.

Both pions produced in untagged $\eta'(958)\to\eta\pi^+\pi^-$ ($\eta\to\gamma\gamma$) events have relatively low momenta, usually less than 200 MeV/c. In the high-field data, the curvature of the pion tracks is so large that they frequently fail even to reach the minimum distance from the beam required if they are to qualify as a track for triggering purposes. Thus it is rare in the low-field data, and nearly impossible in the high-field data, for an untagged $\eta'(958)\to\eta\pi^+\pi^-$ event to satisfy the requirements of the untagged trigger requiring two TPC tracks. Although one of the pions may satisfy the requirements of the trigger requiring one TPC track in coincidence with energy detected in the HEX or PTC, the total energy deposited by the final-state pions and photons in $\eta'(958)$ events is usually insufficient to reach the thresholds above which that trigger will fire. Hence most untagged $\eta'(958)$ events satisfy neither of the untagged triggers described in Sec. III.

Even when one of these events does trigger, the Monte Carlo simulation predicts that it will almost never satisfy

the minimum pion momentum cuts imposed in the $\eta\pi^+\pi^-$ selection procedure described in the previous section. The net result of these losses is that the three $\eta'(958)$ events in the untagged $\eta\pi^+\pi^-$ data are entirely consistent with the number expected, given the existing measurements of $\Gamma_{\gamma\gamma}(\eta')$. Our acceptance for untagged $\eta\pi^+\pi^-$ $(\eta\to\gamma\gamma)$ events, as determined from a Monte Carlo simulation in which the events were evenly distributed over the available phase space, is shown as a function of W in Fig. 3(a).

The corresponding tagged acceptance, shown in Fig. 3(b), is significantly greater at low invariant masses, in accordance with the relatively large $\eta'(958)$ signal seen in Fig. 2(b). The full widths of the 2C-fitted η and 3C-fitted $\eta'(958)$ invariant-mass peaks predicted by the Monte Carlo simulation, about 230 and 30 MeV/c^2, respectively, agree with those observed in the tagged $\eta\pi^+\pi^-$ data. The tagged $\eta'(958)$ mass peak is centered at 961 ± 3 MeV/c^2.

We estimated from the shape of the mass spectrum of Fig. 2(b) that two of the 36 events in the $\eta'(958)$ mass region are background. The Q^2 distribution of the background was taken to be the same as that of events in the high-mass region (above 1350 MeV/c^2) of the singly tagged $\eta\pi^+\pi^-$ spectrum. Figure 4(a) shows the cross section, after subtracting this background, for the reaction $e^+e^-\to e^+e^-\eta'(958)$ with $P^2<0.1$ GeV^2 (where P^2 is defined as in Sec. II) in three bins of Q^2; the corresponding values of the derived quantity $F^2(Q^2)\Gamma_{\gamma\gamma}(\eta')$ defined in Sec. II are shown in Fig. 4(c). That figure also shows our previous measurement of this quantity using the $\pi^+\pi^-\gamma$ decay mode of the $\eta'(958)$ (Ref. 40), and the recent measurement by the Mark II Collaboration based on data in the $\eta\pi^+\pi^-$ channel.[4] The results reported here agree with both these previous experiments, and with the original measurement by the PLUTO Collaboration.[38]

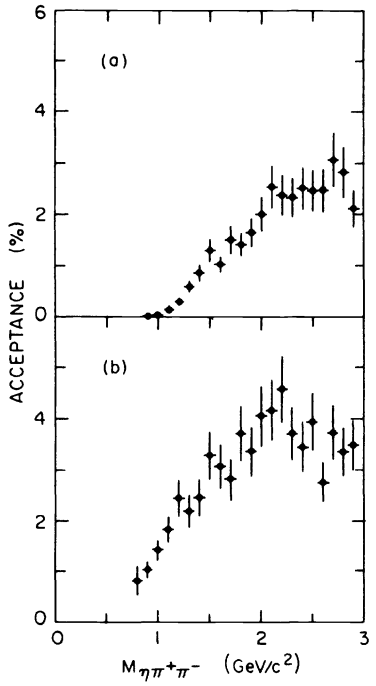

FIG. 3. $\eta\pi^+\pi^-$ $(\eta\to\gamma\gamma)$ acceptances as determined from Monte Carlo simulations: (a) for untagged data and (b) for tagged data.

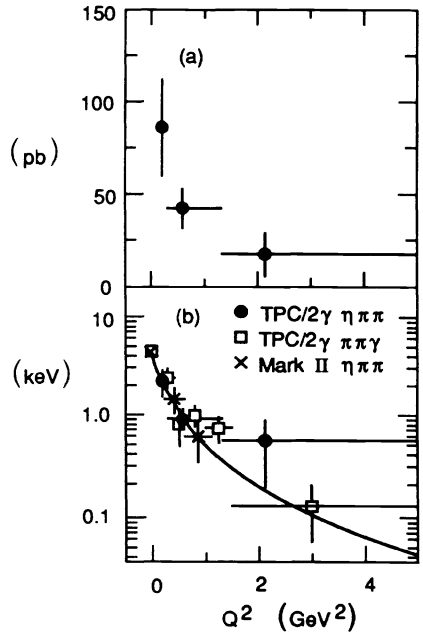

FIG. 4. (a) Total cross sections for $e^+e^-\to e^+e^-\eta'(958)$ with $P^2<0.1$ GeV^2 in various Q^2 bins and (b) $F^2(Q^2)\Gamma_{\gamma\gamma}(\eta')$. Errors shown are statistical only. The curve in (b) is expected if $F=F_\rho$ and $\Gamma_{\gamma\gamma}(\eta')=3.8$ keV. Also shown in (b) are a TPC/Two-Gamma measurement based on the decay $\eta'(958)\to\pi^+\pi^-\gamma$, from Ref. 40, and the Mark II measurement using the $\eta\pi^+\pi^-$ final state, from Ref. 4.

If the virtual photons that fuse to form an $\eta'(958)$ behave as ρ mesons, as suggested by the vector-meson-dominance model,[43] $F^2(Q^2)$ in Eq. (6) might reasonably be given by a ρ form factor, defined by

$$F_\rho^2(Q^2)\equiv\frac{1}{(1+Q^2/M_\rho^2)^2}\ . \tag{12}$$

The limited statistics preclude an accurate determination of $F^2(Q^2)$, but the data are consistent with a ρ form factor. The best fit with $F=F_\rho$ is shown in Fig. 4(b). If this fit is extrapolated to $Q^2=0$, it implies

$$\Gamma_{\gamma\gamma}(\eta')=3.8\pm0.7\pm0.6\ \text{keV}\ . \tag{13}$$

The second error is systematic and includes contributions from uncertainties in the integrated luminosity (5%), the branching fractions involved in the reaction (2%), the simulations of detector response and triggering (5%), and the fraction of events satisfying the selection and fitting procedure (15%).

The value given in Eq. (13) agrees with existing measurements of $\Gamma_{\gamma\gamma}(\eta')$ based on untagged $\eta'(958)$ formation by $\gamma\gamma$ fusion. The Mark II Collaboration found $\Gamma_{\gamma\gamma}(\eta')=4.7\pm0.6+0.9$ keV (Ref. 4) using the untagged $\eta\pi^+\pi^-$ final state, while the Crystal Ball Collaboration found $\Gamma_{\gamma\gamma}(\eta')=4.6\pm0.4\pm0.6$ keV (Ref. 41) using six-

photon data from the $\eta\pi^0\pi^0$ ($\eta\to\gamma\gamma$) decay of the $\eta'(958)$. The same quantity has been measured by a number of groups using untagged data from the decay $\eta'(958)\to\rho^0\gamma\to\pi^+\pi^-\gamma$. The weighted average of the $\Gamma_{\gamma\gamma}(\eta')$ results of the Mark II (SPEAR) (Ref. 35), JADE (Ref. 36), CELLO (Ref. 37), PLUTO (Ref. 38), TASSO (Ref. 39), TPC/Two-Gamma (Ref. 40), and ARGUS (Ref. 42) Collaborations, all of which used comparable models for the $\rho^0\gamma$ decay, is 4.17 ± 0.28 keV, if statistical and systematic errors are combined in quadrature. The agreement of the $\eta'(958)$ results given in this section with previous measurements increases our confidence in the Monte Carlo simulation, which was also used to obtain the $f_1(1285)$ results presented in the next section.

VI. SPIN-ONE MODELS AND $f_1(1285)$ RESULTS

The singly tagged $\eta\pi^+\pi^-$ invariant-mass spectrum shown in Fig. 2(b) has a clear peak containing 26 events, over an estimated background of 8 ± 3 events, centered at a mass of 1273 ± 11 MeV/c^2. There is no corresponding peak in the untagged-data spectrum. As shown in Fig. 3(a), the Monte Carlo simulation predicts significant acceptance for untagged $\eta\pi^+\pi^-$ ($\eta\to\gamma\gamma$) events at this mass, so that such a peak would be expected if the signal in the spectrum of tagged data were due to the formation of a resonance with $J\neq1$. We simulated the formation by $\gamma\gamma$ fusion of an isoscalar, spin-zero resonance $R(1285)$, decaying to $\eta\pi^+\pi^-$ uniformly in three-body phase space. If the branching fraction for the decay of $R(1285)$ to $\eta\pi\pi$ were $B_{\eta\pi\pi}$, and if its $\Gamma^{TT}_{\gamma\gamma^*}(Q^2,W^2)$ were given by Eq. (6) with $F=F_\rho$, then, following a procedure analogous to that used for the $\eta'(958)$, the peak in the spectrum of tagged data would imply $B_{\eta\pi\pi}\Gamma_{\gamma\gamma}(R(1285))\approx2.6$ keV. But if such a resonance existed, there would be a peak near 1285 MeV/c^2 containing approximately 50 events in the spectrum of untagged $\eta\pi^+\pi^-$ data [as shown in Fig. 2(a)]. The observed spectrum cannot accommodate a peak of this size. In fact, given the background estimate shown in Fig. 2(a), and assuming a 17% systematic error, we find $B_{\eta\pi\pi}\Gamma_{\gamma\gamma}(R(1285))<0.6$ keV at the 90% confidence level. This may be interpreted as a limit on the formation of the pseudoscalar state $\eta(1275)$ (Refs. 44 and 45), whose mass and width are comparable to those of the $f_1(1285)$ (Ref. 45). The Crystal Ball Collaboration has set a more stringent limit on the formation of the $\eta(1275)$: using the final state $\eta\pi^0\pi^0$ ($\eta\to\gamma\gamma$), they concluded[41] that $B_{\eta\pi\pi}\Gamma_{\gamma\gamma}(\eta(1275))<0.3$ keV at the 90% confidence level.

It is unlikely that any reasonable model for the formation by $\gamma\gamma$ fusion of a meson with $J\neq1$ could lead to the ratio of untagged to singly tagged events we observe near 1273 MeV/c^2 in the $\eta\pi^+\pi^-$ data. The formation of a spin-one resonance, on the other hand, is expected to be strongly suppressed in untagged data, where both virtual photons have $Q^2\ll W^2$. We therefore conclude that most of the events contributing to the peak in the tagged spectrum represent the formation and subsequent decay into $\eta\pi\pi$ of a spin-one state, possibly the axial-vector meson $f_1(1285)$. To attribute this peak definitely to formation of the $f_1(1285)$, it would be necessary to determine the parity of the state seen in the data. This task is complicated by the fact that the decay angular distributions depend not only on the parity, but also on the size of the cross section for the formation of longitudinally polarized spin-one mesons, relative to that for transversely polarized mesons. As discussed in Sec. II, the ratio of these cross sections is given by the function $\mathcal{R}(Q^2)$. In principle, there are no restrictions on the form of $\mathcal{R}(Q^2)$, except that it must vanish as Q^2 approaches zero for any spin-one meson with a nonzero $\gamma\gamma$ coupling parameter.

The parity of a spin-one meson decaying to three particles influences the distribution of θ^*, which is defined to be the angular separation in the meson's rest frame between the normal to the decay plane and a given polarization axis. We will take this polarization axis to be the direction of the virtual photon momenta in the $\gamma^*\gamma^*$ center of mass. If $\mathcal{R}(Q^2)$ vanished, the expected distribution of $\cos\theta^*$ would then be proportional to $1\pm\cos^2\theta^*$, depending on whether the decaying meson had parity ±1. However, if $\mathcal{R}$ cannot be neglected, the expected distributions are less distinctive. In general, the $\cos\theta^*$ distribution for the decay of a positive-parity state is $1+\cos^2\theta^*+2\mathcal{R}\sin^2\theta^*$; in the negative-parity case, this is replaced by $\sin^2\theta^*+2\mathcal{R}\cos^2\theta^*$.

In the case of the $f_1(1285)$, we can use a model due to Cahn[24] to derive an explicit prediction for $\mathcal{R}(Q^2)$. Cahn's model describes the formation by $\gamma\gamma$ fusion of a nonrelativistic $q\bar{q}$ bound state A with $J^{PC}=1^{++}$. It also predicts the spin-one effective form factor $\tilde{F}(Q^2)$ for such a state; we will use this prediction to extract from our singly tagged data the $\gamma\gamma$ coupling parameters of both the 1273 MeV/c^2 spin-one state discussed here and the 1420-MeV/c^2 spin-one state discussed in Sec. IX. The Cahn model results in the forms

$$\Gamma^{LT}_{\gamma^*\gamma^*}(Q_1^2,Q_2^2,W^2)=\frac{4X}{W^4}\frac{Q_1^2}{W^2}\times F^2(Q_1^2)F^2(Q_2^2)\tilde{\Gamma}_{\gamma\gamma}(A)\,, \tag{14a}$$

$$\Gamma^{TT}_{\gamma^*\gamma^*}(Q_1^2,Q_2^2,W^2)=\frac{4X}{W^4}\frac{(Q_1^2-Q_2^2)^2}{W^4}\times F^2(Q_1^2)F^2(Q_2^2)\tilde{\Gamma}_{\gamma\gamma}(A)\,, \tag{14b}$$

where $\tilde{\Gamma}_{\gamma\gamma}(A)$ is the $\gamma\gamma$-A coupling parameter introduced in Sec. II, and F is a form factor (as yet unspecified) satisfying the normalization condition $F(0)=1$. Because of the convention differences discussed in Sec. II (Ref. 28) these equations contain the factor $4X/W^4$, rather than the factor $(4X/W^4)^{3/2}=8k^3/W^3$ appearing in Ref. 24. Since $\mathcal{L}_{LT}\approx\mathcal{L}_{TT}$ to within about 1% in our Q^2 region, the Cahn model predicts

$$\tilde{F}^2(Q^2,W^2)\approx\left[1+\frac{Q^2}{2W^2}\right]\frac{Q^2}{W^2}F^2(Q^2)\,. \tag{15}$$

The factor $\frac{1}{2}$ in the second term is needed because four virtual-photon polarization states contribute to σ_{TT},

while only two contribute to σ_{LT} [see Eq. (3)]. We refer to the Cahn model prediction for $\mathcal{R}$ as $\mathcal{R}_{\text{Cahn}}$; a comparison of Eqs. (8) and (10) with Eq. (15) yields $\mathcal{R}_{\text{Cahn}}=Q^2/2W^2$.

We have compared the distribution of $\cos\theta^*$ values for the singly tagged $\eta\pi^+\pi^-$ events having invariant masses near the spin-one resonance peak to the expected distributions for positive and negative parities, for both $\mathcal{R}=\mathcal{R}_{\text{Cahn}}$ and $\mathcal{R}=0$. The Kolmogorov-Smirnov statistic[46,47] was used to associate a confidence level with the hypothesis that these data are described by a particular model. This method has the advantage of using all the information available in the $\cos\theta^*$ distribution, independent of binning. Assuming that the background under the resonance is uniformly distributed in $\cos\theta^*$, we found that the observed $\cos\theta^*$ distribution leads to a 69% confidence level for the Cahn-model prediction for a meson with $J^{PC}=1^{++}$; if instead we assume $\mathcal{R}=0$, the positive-parity confidence level is about 29%. The negative-parity confidence levels are roughly 29% and 1.4% for $\mathcal{R}=\mathcal{R}_{\text{Cahn}}$ and $\mathcal{R}=0$, respectively. There is, however, no reason to suppose that either of these choices for $\mathcal{R}(Q^2)$ should correctly describe the formation of a negative-parity resonance (which could not be a $q\bar{q}$ state). Negative parity cannot be excluded if $\mathcal{R}=\mathcal{R}_{\text{Cahn}}$; other possible forms for $\mathcal{R}(Q^2)$ can yield still higher negative-parity confidence levels. On the other hand, at least for these two choices of $\mathcal{R}(Q^2)$, positive parity is preferred.

Since the spin-one state we observe has properties consistent with those of the $f_1(1285)$, we will henceforth assume that the signal at 1273 MeV/c^2 is due to the formation of that meson. Even with this assumption, the number of events in our data is too small to allow us to judge the validity of the application of the Cahn model to the $f_1(1285)$, or to measure the form factor $\tilde{F}^2(Q^2)$. We will nevertheless proceed to use the Cahn model to extract a value for $\tilde{\Gamma}_{\gamma\gamma}(f_1(1285))$ from the tagged $\eta\pi^+\pi^-$ data, by assuming $F=F_\rho$. The decay $f_1(1285)\to\eta\pi\pi$ has been observed[48–50] to proceed primarily via an $a_0(980)\pi$ intermediate state, and we calculated our acceptance using a Monte Carlo program that assumed that decay chain.[51] The 3C-fitted invariant-mass peak resulting from the simulation had a full width of approximately 70 MeV/c^2; both the location and width of the peak were consistent with the signal seen in the singly tagged $\eta\pi^+\pi^-$ data. We defined a signal region extending from 1200 to 1350 MeV/c^2, leading to the estimated numbers of signal and background events given at the beginning of this section. The Q^2 distribution of the background was taken to be the same as that assumed in the analysis of the $\eta'(958)$ signal.

Figure 5(a) shows the cross section for the reaction $e^+e^-\to e^+e^-f_1(1285)$ with $P^2<0.1$ GeV^2 in three bins of Q^2; the average values of $\tilde{F}^2(Q^2)\tilde{\Gamma}_{\gamma\gamma}(f_1(1285))$ to which these cross sections correspond are shown in Fig. 5(b). A fit to the Cahn model with $F=F_\rho$ yields the value

$$\tilde{\Gamma}_{\gamma\gamma}(f_1(1285))=2.4\pm0.5\pm0.5\ \text{keV}\ . \tag{16}$$

The second error is systematic and includes the 12% relative uncertainty in the branching fraction for the decay $f_1(1285)\to\eta\pi\pi$ (Ref. 11); the other contributions are as for the $\eta'(958)$. The curve corresponding to this fit is also shown in Fig. 5(b). Our acceptance in each Q^2 bin is relatively insensitive to changes in the form assumed for $\tilde{F}^2(Q^2)$ in the Monte Carlo simulation; such changes would consequently have little effect on the results presented in Fig. 5(b). On the other hand, fitting with a different $\tilde{F}^2(Q^2)$ could drastically alter the value we obtain for $\tilde{\Gamma}_{\gamma\gamma}(f_1(1285))$; this point will be considered in more detail in Sec. IX, when we discuss our $X(1420)$ results.

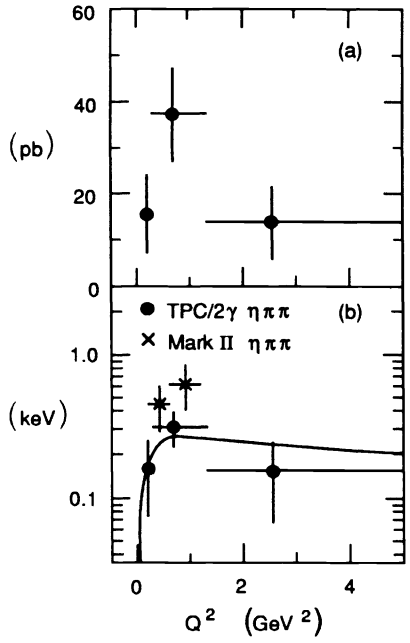

FIG. 5. (a) Total cross sections for $e^+e^-\to e^+e^-f_1(1285)$ with $P^2<0.1$ GeV^2 in various Q^2 bins and (b) $\tilde{F}^2(Q^2)\tilde{\Gamma}_{\gamma\gamma}(f_1(1285))$. Errors shown are statistical only. The curve in (b) is the prediction of the Cahn model with $F=F_\rho$ and $\tilde{\Gamma}_{\gamma\gamma}(f_1(1285))=2.4$ keV. The Mark II results derived (see Ref. 53) from Ref. 4 are also shown in (b).

The value given in Eq. (16) for the $\gamma\gamma$-$f_1(1285)$ coupling parameter is smaller than, but not inconsistent with, the value $4.7\pm1.3\pm0.9$ keV found by the Mark II Collaboration for the same quantity.[4,52] Their results for $\tilde{F}^2(Q^2)\tilde{\Gamma}_{\gamma\gamma}(f_1(1285))$ are shown in Fig. 5(b) (Ref. 53). Since their data all lie in the Q^3 region between 0.2 and 1.2 GeV^2, it is more appropriate to compare their measurement of $\tilde{\Gamma}_{\gamma\gamma}(f_1(1285))$ to the value $2.7\pm0.6\pm0.6$ keV, which best fits our data in a comparable Q^2 region.

VII. ANALYSIS OF THE $\pi^+\pi^-\pi^+\pi^-$ FINAL STATE

We also searched for the formation of $f_1(1285)$ by $\gamma\gamma$ fusion in the $\pi^+\pi^-\pi^+\pi^-$ channel. We selected only events that satisfied one of the triggers described in Sec. III, excluding those requiring energy deposition in the HEX or PTC. We then chose events with exactly four

TPC tracks; two had to be positively, and the other two negatively charged. Each track was required to have $\chi_\pi^2 < 8$. One track had to have $\chi_\pi^2 + 2 < \min(\chi_e^2, \chi_K^2, \chi_p^2)$, so that it was unlikely to have been left by anything other than a pion. Other cuts excluded events consistent with being $K^+K^-\pi^+\pi^-$ or $K^\pm K_S^0\pi^\mp$ ($K_S^0 \to \pi^+\pi^-$). The tracks were also also required to (1) have momenta greater than 120 MeV/c, (2) be at least 350 mrad from the beam, (3) have a relative momentum error of less than 30%, and (4) be consistent with having originated near the interaction point. To select exclusive events, we required that the magnitude of the total transverse momentum of the four pions (and the tag, if any) be less than 200 MeV/c. Tags were required to have deposited at least 4 GeV in the NaI or SHW calorimeters. All the tagged data were scanned to reject improperly reconstructed events.

Figure 6 shows invariant-mass spectra of the final

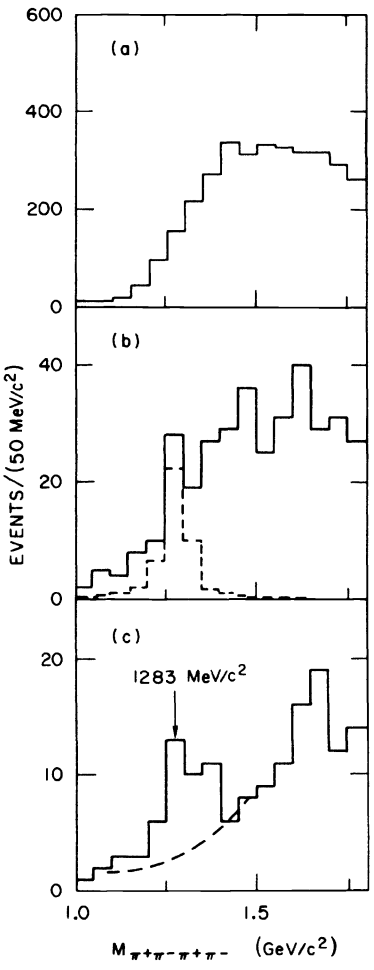

FIG. 6. Invariant-mass spectra of $\pi^+\pi^-\pi^+\pi^-$ events: (a) untagged data, (b) tagged data, and (c) tagged data with $Q^2 > 0.5$ GeV^2. The dashed histogram in (b) shows the contribution expected from $f_1(1285)$ formation if $\tilde{\Gamma}_{\gamma\gamma}(f_1(1285)) = 2.4$ keV and the $f_1(1285)$ effective form factor $\tilde{F}^2(Q^2)$ has the form predicted by the Cahn model with $F = F_\rho$. The dashed line in (c) represents the background estimate used to derive the upper limit given in Sec. VII.

$\pi^+\pi^-\pi^+\pi^-$ event sample, for untagged data [Fig. 6(a)], tagged data [Fig. 6(b)], and tagged data with $Q^2 > 0.5$ GeV^2 [Fig. 6(c)]. There is no peak in the untagged data near 1285 MeV/c^2, but in the tagged data there is some sign of a resonance in that vicinity. We simulated formation of $f_1(1285)$ using the Monte Carlo program described in Sec. VI, but now with the decay chain $f_1(1285) \to \rho^0\pi^+\pi^- \to \pi^+\pi^-\pi^+\pi^-$ (Ref. 49). Since the proximity of the $\rho^0\rho^0$ threshold enhancement renders our background estimate quite uncertain, we used our $\pi^+\pi^-\pi^+\pi^-$ data only to determine an upper limit on $f_1(1285)$ formation.

To do this, we used the mass spectrum shown in Fig. 6(c); the dashed curve shown there represents what we consider to be a conservatively low estimate of the background beneath an $f_1(1285)$ peak. If the $\pi\pi\pi\pi$ decays of the $f_1(1285)$ all proceed via the intermediate state $\rho\pi\pi$, then $\frac{1}{3}$ of those decays will lead to the $\pi^+\pi^-\pi^+\pi^-$ final state, resulting in a net branching fraction of $(13.3 \pm 2.0)\%$ for the decay $f_1(1285) \to \pi^+\pi^-\pi^+\pi^-$. With this assumption, which was used in the determination of the $f_1(1285)$ branching fractions quoted in Sec. IV, and taking the background to be that shown in Fig. 6(c), we found that the tagged $\pi^+\pi^-\pi^+\pi^-$ data imply $\tilde{\Gamma}_{\gamma\gamma}(f_1(1285)) < 2.4$ keV at the 90% confidence level. This limit, though relatively low, is consistent with our measurement based on the $\eta\pi^+\pi^-$ channel, particularly considering the strong negative correlation between the fitted $\pi\pi\pi\pi$ and $\eta\pi\pi$ branching fractions[11] [a consequence of the fact that the measured quantity is the ratio $B(f_1(1285) \to \eta\pi^+\pi^-)/B(f_1(1285) \to \pi^+\pi^-\pi^+\pi^-)$]. The dashed histogram in Fig. 6(b) represents the expected contribution to the invariant-mass spectrum of tagged $\pi^+\pi^-\pi^+\pi^-$ data from the process $\gamma^*\gamma^* \to f_1(1285) \to \pi^+\pi^-\pi^+\pi^-$, given these branching fractions and the $\gamma\gamma$-$f_1(1285)$ coupling parameter determined from our singly-tagged $\eta\pi^+\pi^-$ data.

VIII. ANALYSIS OF THE $K^\pm K_S^0\pi^\mp$ FINAL STATE

We have previously reported[1] evidence for the formation by $\gamma\gamma$ fusion of a spin-one meson whose invariant mass is near 1420 MeV/c^2. It was observed in the final state $K^\pm K_S^0\pi^\mp$ ($K_S^0 \to \pi^+\pi^-$). We have reanalyzed the formation of this resonance, which we call the $X(1420)$, including new data, the analysis of which was incomplete at the time of our original report. These additional data, taken with the superconducting coil, represent about 25% of the total integrated luminosity reported in Sec. III.

The triggers used in selecting a $K^\pm\pi^\mp\pi^+\pi^-$ event sample were the same as those used in the $\pi^+\pi^-\pi^+\pi^-$ case. The kaon-candidate tracks had to have $\chi_K^2 < 8$ and $\chi_K^2 + 2 < \min(\chi_e^2, \chi_\pi^2, \chi_p^2)$. Each of the four tracks was required to satisfy the same track-quality requirements imposed in the $\pi^+\pi^-\pi^+\pi^-$ analysis described above. Since low-momentum kaons cannot penetrate the material between the interaction point and the TPC, we required that the momenta of the kaon-candidate tracks be greater than 310 MeV/c. The other three tracks in each event

were required to be consistent with pions; specifically, they had to have either $\chi_\pi^2 < 8$ or $\chi_\pi^2 + 2 < \min(\chi_e^2, \chi_K^2, \chi_p^2)$. To reduce background from $K^+K^-\pi^+\pi^-$ events, the two tracks with charge opposite to the kaon candidate had to have $\chi_K^2 > 4$. As in the $\pi^+\pi^-\pi^+\pi^-$ analysis, tags were required to deposit at least 4 GeV in the NaI or SHW calorimeters. To select exclusive events, we then required that the magnitude of the total transverse momentum of each event, including the tag (if any), be less than 250 MeV/c.

We next searched for $\pi^+\pi^-$ pairs resulting from K_S^0 decays. This was done by requiring that the $\pi^+\pi^-$ invariant mass, calculated using the pion four-momenta at the point of closest approach of the two tracks, be within 45 MeV/c^2 of the K_S^0 mass (70 MeV/c^2 in the low-field data). These $K^\pm K_S^0 \pi^\mp$ ($K_S^0 \to \pi^+\pi^-$) candidates were scanned to remove events with evidence of additional low-angle tracks or low-energy photons. The invariant $K^\pm K_S^0 \pi^\mp$ masses of the remaining events were then obtained by scaling the momenta of the pions identified as coming from a K_S^0 decay so that $M_{\pi^+\pi^-} = M_{K^0}$ (Ref. 54). The resulting untagged and tagged $K^\pm K_S^0 \pi^\mp$ mass spectra are shown in Fig. 7. While there is no peak near 1420 MeV/c^2 in the invariant-mass spectrum of untagged data, the peak corresponding to the $X(1420)$ is apparent in the tagged-data spectrum. This observation, together with Monte Carlo calculations of our tagged and untagged $K^\pm K_S^0 \pi^\mp$ ($K_S^0 \to \pi^+\pi^-$) acceptances, led to our conclusion in Ref. 1 that the $X(1420)$ is a spin-one state.

Before proceeding with the analysis of the $X(1420)$, we return briefly to the $f_1(1285)$. As noted in Sec. IV, the $f_1(1285)$ decays $(11\pm3)\%$ of the time to $K\bar{K}\pi$. A Monte Carlo simulation of this decay resulted in an $f_1(1285)$ mass peak in the $K^\pm K_S^0 \pi^\mp$ ($K_S^0 \to \pi^+\pi^-$) channel with a full width of 41 MeV/c^2. If $\tilde{\Gamma}_{\gamma\gamma}(f_1(1285))$ is 2.4 keV, as obtained from the $\eta\pi^+\pi^-$ analysis, the simulation predicts three $f_1(1285)$ events in the tagged $K^\pm K_S^0 \pi^\mp$ data. This prediction is consistent with the observed mass spectrum shown in Fig. 7(b).

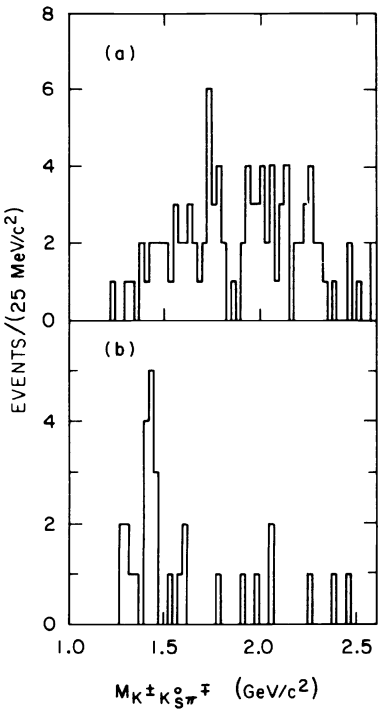

FIG. 7. Invariant-mass spectra of $K_S^0 K^\pm \pi^\mp$ events: (a) untagged data and (b) tagged data.

To continue our analysis of the $X(1420)$, we excluded doubly tagged events, as well as singly tagged events in which the tag failed fiducial cuts made to ensure that Q^2 was measured accurately. Events with masses between 1330 and 1520 MeV/c^2 were used to measure a resonance mass of 1426^{+11}_{-7} MeV/c^2. We assumed a flat background of 1.2 events per 100 MeV/c^2, but the mass obtained was not particularly sensitive to this assumption. Both this mass and the width of the peak are consistent with the values expected for the $f_1(1420)$. For purposes of measuring quantities strongly influenced by the amount of background, we used only events whose invariant masses lie in a narrower mass range, extending from 1390 to 1470 MeV/c^2. This cut resulted in a final sample of nine events, one of which we assume to be background. Monte Carlo simulations imply that the minimum W cut at 1390 MeV/c^2 excludes most $f_1(1285)$ mesons.

IX. $X(1420)$ RESULTS

We turn next to the question of whether or not the $X(1420)$ is the $f_1(1420)$ seen in hadronic interactions. That state decays to $K\bar{K}\pi$, the decay proceeding primarily[15] through a $K^*(892)K$ intermediate state.[55] The Dalitz plot in Fig. 8 shows the squared $K\pi$ invariant masses of the nine events in the $X(1420)$ signal region. Given our estimated background of one event, we conclude from the Dalitz plot that the $X(1420)$ mesons could all have decayed via the $K^*(892)K$ channel.

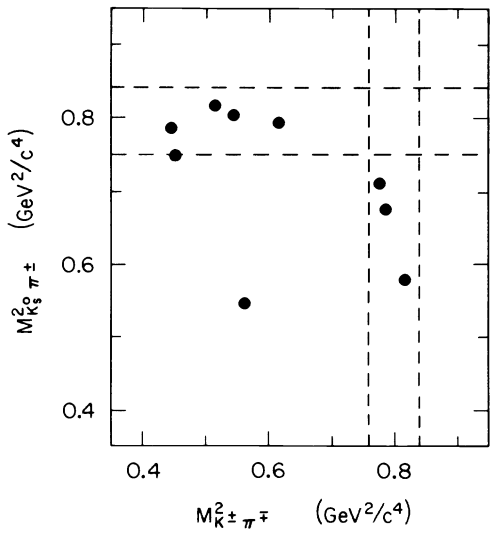

FIG. 8. Scatter plot relating the two $K\pi$ invariant masses in the $K_S^0 K^\pm \pi^\mp$ final state. The dashed lines enclose $K^{*0}(892)$ and $K^{*\pm}(896)$ bands. The bands are centered at $M^2_{K^*}$ and have have a width of $2M_{K^*}\Gamma_{K^*}$.

Spin-one mesons formed by $\gamma\gamma$ fusion must have either $J^{PC}=1^{++}$, as does the $f_1(1420)$, or $J^{PC}=1^{-+}$. A state with $J^{PC}=1^{-+}$ cannot be a conventional $q\bar{q}$ meson, and might be a $q\bar{q}g$ hybrid.[22] The parity of the $X(1420)$ is therefore an important clue to its identity. Since the parity of a state decaying to three particles manifests itself in the decay angular distributions, we considered the Dalitz plot of our $X(1420)$ data shown in Fig. 9(a). Figure 9(b), a scatter plot resulting from a Monte Carlo simulation of a spin-zero resonance decaying uniformly in three-body phase space, demonstrates that our acceptance is essentially flat in the Dalitz-plot variables. But a spin-one particle with negative parity should have its decay rate suppressed near the kinematic boundary, where the momenta are collinear in the $X(1420)$ rest frame. Figure 9(a) shows that there is no such suppression unless it occurs only very near the boundary, so that greatly increased statistics would be required to observe it.

This qualitative argument therefore suggests that the parity is positive. But other effects might obscure the suppression of negative-parity $X(1420)$ events near the kinematic boundary. For example, if the $X(1420)$ decays via $K^*(892)K$, then the presence of $K^*(892)$ bands near the edges of the Dalitz plot would tend to compensate for the reduction in event density otherwise expected there. Moreover, the angular distribution resulting from the decay of a $J^{PC}=1^{-+}$ meson with helicity zero would increase the density of events in some regions near the kinematic boundary. By helicity zero, we mean that the meson has no spin projection along the direction of the virtual photon momenta in the $\gamma^*\gamma^*$ center of mass: helicity-zero mesons are produced by the σ_{TT} term in Eq. (2); the influence of such events on the Dalitz plot therefore depends on the function $\mathcal{R}(Q^2,W^2)$ defined in Eq. (9).

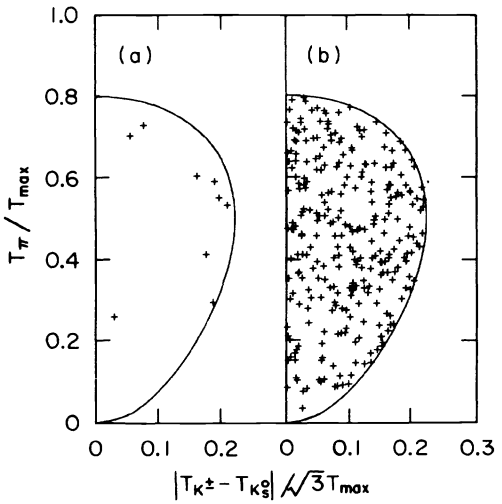

FIG. 9. Dalitz plots of (a) events in the $X(1420)$ peaks after application of all selection criteria and (b) Monte Carlo events simulated using a model of a spin-zero resonance at 1420 MeV/c^2, decaying uniformly in three-body $K^\pm K^0_S \pi^\mp$ phase space. T_i is the kinetic energy of particle type i, and T_{max} is the total kinetic energy in the event.

To make these considerations more quantitative, we used the Kolmogorov-Smirnov statistic[46,47] to determine confidence levels for the observed $X(1420)$ mesons to have undergone decays described by a variety of possible matrix elements. If the $X(1420)$ has positive parity, the decay matrix element must be the dot product of the $X(1420)$ polarization vector $\mathbf{e}_X$ with a linear combination of $\mathbf{p}_\pi$ and $\mathbf{p}_K$, the momenta of the pion and the charged kaon in the $X(1420)$ rest frame. The coefficients of $\mathbf{p}_\pi$ and $\mathbf{p}_K$ must be Lorentz-scalar functions of the four-momenta of the decay particles. If the parity is negative, the decay matrix element must instead be equal to such a function times $\mathbf{e}_X\cdot(\mathbf{p}_\pi\times\mathbf{p}_K)$.

In either case, the value of a matrix element for a given event depends not only on $\mathbf{e}_X$ [i.e., whether the $X(1420)$ was produced by the σ_{TT} or σ_{LT} term in Eq. (2)], but also on whether the decay proceeds via a resonant intermediate state, such as $K^*(892)K$ or $a_0(980)\pi$. In the positive-parity case, the linear combination of $\mathbf{p}_\pi$ and $\mathbf{p}_K$ appearing in the matrix element depends on whether the K^0_S is in an S-wave or D-wave state, or a mixture of the two, relative to the $K^\pm\pi^\mp$ system.

We found reasonably high confidence levels for many of the matrix elements considered. In particular, there was a 70% confidence level for the matrix element corresponding to an $L=0$ $K^*(892)K$ decay of a $J^{PC}=1^{++}$ meson with $\mathcal{R}(Q^2)$ as specified by the Cahn model. The authors of Ref. 15 found that this decay most closely matched their $f_1(1420)$ data. Although the confidence levels for the negative-parity matrix elements we tried were 6.5% or less if we assumed $\mathcal{R}=0$, larger σ_{TT} contributions led to much higher confidence levels. So, while the $X(1420)$ decays in a manner consistent with the observed behavior of the $f_1(1420)$, the matrix element analysis cannot exclude other possibilities, including some corresponding to negative parity.

The distribution of $\cos\theta^*$, where the angle θ^* is defined as in Sec. VI, can be used to distinguish between positive and negative parity independent of the decay dynamics. As noted in Sec. VI, the expected distribution depends on the function $\mathcal{R}(Q^2,W^2)$. We consider here two possibilities: $\mathcal{R}=0$ and $\mathcal{R}=\mathcal{R}_{\text{Cahn}}$, where $\mathcal{R}_{\text{Cahn}}=Q^2/2W^2$. If $\mathcal{R}=\mathcal{R}_{\text{Cahn}}$, the Kolmogorov-Smirnov statistic for the observed distribution of $\cos\theta^*$ values results in a 36% confidence level for positive parity, versus 19% for negative parity. If $\mathcal{R}=0$ we find a 63% confidence level for positive parity, and a slightly less than 3% confidence level for negative parity. The $\cos\theta^*$ distribution cannot be used to exclude negative parity for the $X(1420)$ if $\mathcal{R}$ is large. If we consider only the seven events with $Q^2<1.5$ GeV^2, where $\mathcal{R}$ is likely to be smaller than at high Q^2, the negative-parity angular distribution has a confidence level below 6% if $\mathcal{R}=\mathcal{R}_{\text{Cahn}}$, and below 3% if $\mathcal{R}=0$. Using only these events, the positive-parity confidence levels become 39% for $\mathcal{R}=\mathcal{R}_{\text{Cahn}}$, and 56% for $\mathcal{R}=0$. Other possible forms for the function $\mathcal{R}(Q^2)$, which result in considerably higher negative-parity confidence levels, cannot be excluded even for $Q^2<1.5$ GeV^2. As discussed in Sec. II, $\mathcal{R}(Q^2)$ must vanish as Q^2 approaches zero for any spin-

one resonance with a nonzero $\gamma\gamma$ coupling parameter; however, the Q^2 values we observe are too large to justify the assumption $\mathcal{R}=0$ on that basis. With regard to $\mathcal{R}_{\text{Cahn}}$, it should be noted that the Cahn model was derived specifically for positive-parity $q\bar{q}$ mesons; no comparable model has been proposed for the formation by $\gamma\gamma$ fusion of an exotic state with $J^{PC}=1^{-+}$. In view of the negative-parity confidence levels given above, as well as the theoretical uncertainty in the form of $\mathcal{R}(Q^2)$ for a negative-parity spin-one state, we cannot prove that the $X(1420)$ is the $f_1(1420)$, though the decay distributions are all consistent with that identification.

We have also used the $X(1420)$ signal to measure its $\Gamma_{\gamma\gamma^*}(Q^2)$. Our experimental acceptance was determined by simulating the formation by $\gamma\gamma$ fusion of a spin-one resonance at 1420 MeV/c^2, decaying via a $K^*(892)K$ intermediate state to $K^{\pm}K_S^0\pi^{\mp}$, and thence to $K^{\pm}\pi^{\mp}\pi^+\pi^-$. The model used to describe its formation and the simulation of detector response and triggering were identical to those used for the $f_1(1285)$, including the assumption of $\tilde{F}^2(Q^2)$ as specified by the Cahn model with $F=F_\rho$. We denote the unknown branching fraction for the decay of $X(1420)$ to $K\bar{K}\pi$ by $B_{K\bar{K}\pi}$. The $f_1(1420)$ has not been observed to decay via any channel other than $K\bar{K}\pi$, so if the $X(1420)$ is the $f_1(1420)$, $B_{K\bar{K}\pi}$ is probably large. We assumed that roughly 23% of the $K\bar{K}\pi$ decays lead to a $K^{\pm}\pi^{\mp}\pi^+\pi^-$ final state, which is correct if the $X(1420)$ is an isoscalar, and, in particular, if it is the $f_1(1420)$.

Figure 10(a) shows the cross section for the reaction $e^+e^-\to e^+e^-X(1420)\to e^+e^-K\bar{K}\pi$ with $P^2<0.1$ GeV^2 in three bins of Q^2; the corresponding average values of $B_{K\bar{K}\pi}\tilde{F}^2(Q^2)\tilde{\Gamma}_{\gamma\gamma}(X(1420))$ are shown in Fig. 10(b). These results are relatively independent of details of the Monte Carlo model. For example, if we change the Monte Carlo program to use $F=F_\phi$ [where the ϕ form factor F_ϕ is defined by substituting ϕ for ρ in Eq. (12)] rather than $F=F_\rho$, the acceptances used in making Fig. 10 change by less than 3%. The value of $B_{K\bar{K}\pi}\tilde{\Gamma}_{\gamma\gamma}(X(1420))$ implied by these data, however, depends strongly on the choice of form factor:

$$B_{K\bar{K}\pi}\tilde{\Gamma}_{\gamma\gamma}(X(1420))=\begin{cases}1.3\pm0.5\pm0.3\text{ keV} & \text{if } F=F_\rho\ ,\\ 0.63\pm0.24\pm0.15\text{ keV} & \text{if } F=F_\phi\ .\end{cases} \tag{17}$$

The curves corresponding to these fits are also shown in Fig. 10(b). The Mark II Collaboration, using the assumption $F=F_\rho$, found $B_{K\bar{K}\pi}\tilde{\Gamma}_{\gamma\gamma}(X(1420))=1.65\pm0.7\pm0.3$ keV (Refs. 2 and 52). That result should be compared to the value $1.5\pm0.6\pm0.4$ keV, which was obtained from our data in a Q^2 region comparable to the 0.2–1.1 GeV^2 range used by the Mark II group.

The model used in Ref. 1 omitted the factor $4X/W^4$ in Eq. (10) and assumed $\mathcal{R}=0$, rather than $\mathcal{R}=\mathcal{R}_{\text{Cahn}}$. If we were to use that model here, the values given in Eq. (17) would increase by a factor of 2.9. Conversely, the $6\pm2\pm2$ keV result for $B_{K\bar{K}\pi}\tilde{\Gamma}_{\gamma\gamma}(X(1420))$ given in Ref. 1 would become $2.1\pm0.7\pm0.7$ keV using our present model. The remaining difference between this value and the $1.3\pm0.5\pm0.3$ keV given in Eq. (17) is due to addition to the new data and to changes in analysis cuts and scanning procedures relative to those described in Ref. 1. These changes, designed to suppress backgrounds more effectively, included making tighter W cuts and rejecting more events because of the presence of isolated, but low-energy, calorimeter showers.

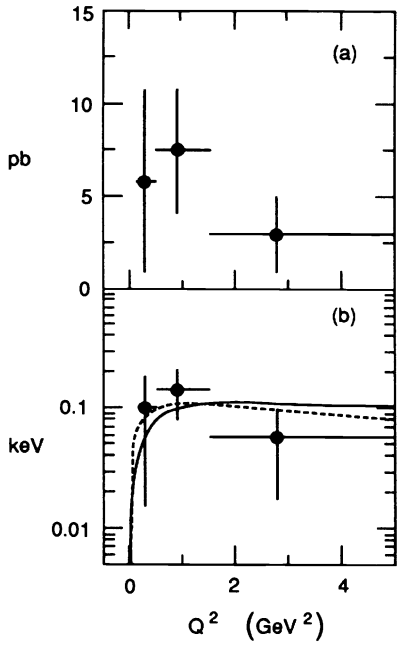

FIG. 10. (a) Total cross sections for $e^+e^-\to e^+e^-X(1420)\to e^+e^-K\bar{K}\pi$ with $P^2<0.1$ GeV^2 in various Q^2 bins and (b) $B_{K\bar{K}\pi}\tilde{F}^2(Q^2)\tilde{\Gamma}_{\gamma\gamma}(X(1420))$. Errors shown are statistical only. The curves shown in (b) are the predictions of the Cahn model with different form factors: the solid curve is its prediction if $F=F_\phi$ and $B_{K\bar{K}\pi}\tilde{\Gamma}_{\gamma\gamma}(X(1420))=0.63$ keV; the dashed curve is its prediction if $F=F_\rho$ and $B_{K\bar{K}\pi}\tilde{\Gamma}_{\gamma\gamma}(X(1420))=1.3$ keV.

It should be noted that the results given in Eq. (17) were derived in the context of the Cahn model for the formation of axial-vector $q\bar{q}$ mesons. If suggestions that the $X(1420)$ is a $q^2\bar{q}^2$ or $q\bar{q}g$ state are correct, its effective form factor $\tilde{F}^2(Q^2)$ may be different from those predicted by the Cahn model. If this is so, $B_{K\bar{K}\pi}\tilde{\Gamma}_{\gamma\gamma}(X(1420))$ could be considerably different from the values given in Eq. (17).

X. MIXING IN THE AXIAL-VECTOR MESON NONET

A spin-one meson's $\gamma\gamma$ coupling parameter, like the $\gamma\gamma$ partial width of a pseudoscalar or tensor meson, is related to its quark content. If the meson is one of the two isoscalar members of a $q\bar{q}$ meson nonet, its quark content depends in turn on the mixing between the SU(3)-singlet and -octet states. In this section, we consider the axial-vector-meson nonet: if θ_A is the mixing angle between its singlet and octet components, then

$$|f_1\rangle = \sin\theta_A\,|f_1^{\text{octet}}\rangle + \cos\theta_A\,|f_1^{\text{singlet}}\rangle\ ,$$
$$|f_1'\rangle = \cos\theta_A\,|f_1^{\text{octet}}\rangle - \sin\theta_A\,|f_1^{\text{singlet}}\rangle\ . \tag{18}$$

The f_1 state is usually identified with the $f_1(1285)$, and the f_1' is the other isoscalar member of the nonet. As discussed in Sec. I, the f_1' is probably a mostly $s\bar{s}$ state; both the $f_1(1420)$ and the $f_1(1530)$ have been advanced as f_1' candidates.

The $X(1420)$, as far as we can determine, has properties consistent with those of the $f_1(1420)$. We now consider whether the identification of the $X(1420)$ with the f_1' is compatible with the values for $\tilde{\Gamma}_{\gamma\gamma}(f_1(1285))$ and $B_{K\bar{K}\pi}\tilde{\Gamma}_{\gamma\gamma}(X(1420))$ given in Secs. VI and IX. To do this, we suppose that the $X(1420)$ is the f_1', and that the radial wave functions of the singlet and octet states in that nonet have approximately equal derivatives at the origin.[56] We then use our measurements of the $\gamma\gamma$-$f_1(1285)$ and $\gamma\gamma$-$X(1420)$ coupling parameters, with the assumption $B_{K\bar{K}\pi}\approx 1$, to determine θ_A. In an ideally mixed nonet, corresponding to $\theta_A=\arcsin 1/\sqrt{3}\approx 35.3°$, the f_1' would be a pure $s\bar{s}$ state. The Gell-Mann–Okubo quadratic mass formula, given an f_1' mass of 1420 MeV/c^2 and a K_1 mass of 1340 MeV/c^2 (Ref. 57), results in a slightly larger mixing angle, $\theta_A\approx 42.2°$.

It has already been noted that the $\tilde{\Gamma}_{\gamma\gamma}$ values presented in Secs. VI and IX are sensitive to the choice of form factor in the Cahn model. In this section, we use the symbols $\tilde{F}_\rho$ and $\tilde{F}_\phi$ to refer to the spin-one effective form factors $\tilde{F}(Q^2,W^2)$ predicted by the Cahn model with $F=F_\rho$ and $F=F_\phi$ [see Eq. (15)]. We have assumed in this analysis that the choice $\tilde{F}=\tilde{F}_\rho$ is appropriate for the $f_1(1285)$. This is probably a reasonable assumption if, as indicated by its mass and decay branching fractions, its $s\bar{s}$ content is small. We will, however, consider both $\tilde{F}=\tilde{F}_\rho$ and $\tilde{F}=\tilde{F}_\phi$ as possibilities for the $X(1420)$.

As stated in Sec. I, the most reliable way to determine θ_A is to compare $\tilde{\Gamma}_{\gamma\gamma}(f_1(1285))$ and $\tilde{\Gamma}_{\gamma\gamma}(f_1')$. We will discuss such a comparison later in this section. But first, we consider the consequences of making, in addition to the assumptions described above, the more dubious assumption that the radial wave functions of the $^3P_2$ tensor-meson nonet and the $^3P_1$ axial-vector-meson nonet are the same. If this is so, θ_A can be determined by comparing the $\gamma\gamma$-$f_1(1285)$ and $\gamma\gamma$-f_1' coupling parameters to $\Gamma_{\gamma\gamma}(f_2(1270))$ (Refs. 56 and 24). In the case of the f_1', the relevant relation is

$$\frac{\tilde{\Gamma}_{\gamma\gamma}(f_1')}{\Gamma_{\gamma\gamma}(f_2(1270))}=\frac{5}{6}\frac{M_1'}{M_2}\frac{\sin^2(\theta_A-\theta_0)}{\cos^2(\theta_T-\theta_0)}\ , \tag{19}$$

where $\theta_T\approx 28°$ is the mixing angle of the $J^{PC}=2^{++}$ tensor-meson nonet as computed from the Gell-Mann–Okubo quadratic mass formula, and $\theta_0=\arcsin\frac{1}{3}\approx 19.5°$ is the mixing angle for which the $\gamma\gamma$-f_1' coupling vanishes. The symbols M_1, M_1', and M_2 represent the masses of the f_1, f_1', and f_2, respectively. The ratios of masses in this and subsequent formulas express the relative amounts of S-wave phase space available for the reactions compared, when both photons are nearly real.[58]

With $M_1'=1420$ MeV/c^2, $M_2=1270$ MeV/c^2, and $\Gamma_{\gamma\gamma}(f_2(1270))=2.70$ keV (Refs. 11 and 59), Eq. (19) implies

$$\sin^2(\theta_A-\theta_0)=\frac{\tilde{\Gamma}_{\gamma\gamma}(f_1')}{2.57\text{ keV}}\ . \tag{20}$$

Using this equation, the ideal mixing angle and the mixing angle implied by the Gell-Mann–Okubo quadratic mass formula result in values for $\tilde{\Gamma}_{\gamma\gamma}(f_1')$ of 0.19 keV and 0.38 keV, respectively. Both are smaller than either of the values given in Eq. (17) for $B_{K\bar{K}\pi}\tilde{\Gamma}_{\gamma\gamma}(X(1420))$, and hence must be smaller than the corresponding values of $\tilde{\Gamma}_{\gamma\gamma}(X(1420))$, even if $B_{K\bar{K}\pi}$ is unity.

A comparison of $f_1(1285)$ to $f_2(1270)$ yields the analog of Eq. (20):

$$\cos^2(\theta_A-\theta_0)=\frac{\tilde{\Gamma}_{\gamma\gamma}(f_1(1285))}{2.33\text{ keV}}\ . \tag{21}$$

In this case, ideal mixing and the Gell-Mann–Okubo mixing angle correspond to $\tilde{\Gamma}_{\gamma\gamma}(f_1(1285))$ values of 2.15 and 1.97 keV, respectively. These are both consistent with our measured value of $2.4\pm0.5\pm0.5$ keV. Since our experimentally determined values of $\tilde{\Gamma}_{\gamma\gamma}$ for both spin-one states are sensitive to changes in the spin-one model, the mixing angles implied by Eqs. (20) and (21) are also sensitive to such changes.

There is less theoretical and experimental uncertainty in a quark-model prediction relating the $\gamma\gamma$ coupling parameters of two mesons within the same nonet. Such a relation between $\tilde{\Gamma}_{\gamma\gamma}(f_1(1285))$ and $\tilde{\Gamma}_{\gamma\gamma}(f_1')$ is

$$\frac{\tilde{\Gamma}_{\gamma\gamma}(f_1(1285))}{\tilde{\Gamma}_{\gamma\gamma}(f_1')}=\frac{M_1}{M_1'}\cot^2(\theta_A-\theta_0)\ . \tag{22}$$

To make use of this equation, we assume $B_{K\bar{K}\pi}=1$; if it were smaller, the value of $\tilde{\Gamma}_{\gamma\gamma}(X(1420))$ implied by our tagged $K^\pm K_S^0\pi^\mp$ data would be larger, and the mixing angles determined below would change accordingly. If this assumption is correct, and if the $X(1420)$ is the f_1', then the results given in Eqs. (16) and (17) for $F=F_\rho$ imply that the ratio appearing on the left hand side of Eq. (22) is $1.8^{+1.6}_{-0.7}$, (Ref. 60), which yields $\theta_A=54.4\pm7.5$ degrees. Alternatively, if λ is defined by

$$|f_1'\rangle=\cos\lambda\,|s\bar{s}\rangle-\sin\lambda\left[\frac{|u\bar{u}\rangle+|d\bar{d}\rangle}{\sqrt{2}}\right]\ , \tag{23}$$

we find $\lambda=(-19.2\pm7.5)°$. The Mark II Collaboration, also assuming $\tilde{F}=\tilde{F}_\rho$ but using a slightly different version of Eq. (22) (Refs. 58 and 61), reported that their measurements of the coupling parameters implied $\lambda=(-15^{+5}_{-10})°$, in agreement with our value.

Equation (22) has a second solution, with $\theta_A=-15.5°$, which corresponds to $\lambda=50.7°$. That would describe an isoscalar member of the axial-vector-meson nonet composed more of $(u\bar{u}+d\bar{d})/\sqrt{2}$ than of $s\bar{s}$. This seems un-

likely if the f_1' is the $f_1(1420)$, since the $f_1(1420)$ is heavier than the $f_1(1285)$ and decays to $K\bar{K}\pi$ and not to $\eta\pi\pi$ (Ref. 45), whereas an f_1' with a $u\bar{u}+d\bar{d}$ content as large as that predicted by the second solution should decay a substantial fraction of the time to final states like $\pi\pi\pi\pi$ and $\eta\pi\pi$. Indeed, the fact that a $q\bar{q}$ meson which is not dominantly $s\bar{s}$ would be expected to decay via these channels implies that the second solution is likely to be internally inconsistent with our assumption that $B_{K\bar{K}\pi}\approx 1$. The second solution would also imply that the $f_{1(1285)}$ is more than 50% $s\bar{s}$: this is contrary to the usual assumption, based on its mass and decay branching fractions, that the $f_1(1285)$ is primarily composed of nonstrange quarks.

If, as is generally assumed, the f_1' is mostly $s\bar{s}$, its true $\tilde{F}$ may well be more similar to $\tilde{F}_\phi$ than to $\tilde{F}_\rho$. If we assume $\tilde{F}=\tilde{F}_\phi$ for the $X(1420)$ [but not for the $f_1(1285)$], the ratio of $\tilde{\Gamma}_{\gamma\gamma}(f_1(1285))$ to $\tilde{\Gamma}_{\gamma\gamma}(X(1420))$ becomes $3.8^{+3.2}_{-1.5}$ (Ref. 60). Equation (22) then leads to the result $\theta_A=(45.4\pm 6.2)°$, which corresponds to $\lambda=(-10.2\pm 6.2)°$. This is quite close to the 42.2° predicted by the Gell-Mann–Okubo quadratic mass formula, for which the ratio $\tilde{\Gamma}_{\gamma\gamma}(f_1(1285))/\tilde{\Gamma}_{\gamma\gamma}(f_1')$ would have the value 5.1. Once again there is a second solution, which we reject on the same grounds as before.

It is difficult to reconcile our $X(1420)$ results with the hypothesis that the $X(1420)$ is the f_1' in an ideally mixed nonet, since Eq. (22) would then imply that $\tilde{\Gamma}_{\gamma\gamma}(f_1(1285))$ should be 11.3 times greater than $\tilde{\Gamma}_{\gamma\gamma}(X(1420))$. However, if the mixing angle is 45.4°, the composition of the f_1' would still be 97% $s\bar{s}$, and only 3% $u\bar{u}$ and $d\bar{d}$. Our data are thus consistent with the identification of the $X(1420)$ as a mostly-$s\bar{s}$ f_1'. However, we cannot rule out scenarios in which the $X(1420)$ does not belong to the axial-vector-meson nonet. If the $X(1420)$ is an exotic state, we could not use the value of $\tilde{\Gamma}_{\gamma\gamma}(X(1420))$ to determine its quark content unless the form of the $X(1420)$ wave function were known.

XI. SUMMARY

We have observed the formation of two spin-one resonances in $\gamma\gamma$ fusion reactions. We concluded that both mesons have $J=1$ because there was evidence of their formation only in tagged interactions, in which one of the interacting photons had $Q^2>0.1$ GeV^2, with Q^2 defined as the negative of the virtual-photon invariant mass squared. Mesons with $J\neq 1$ would also have been formed in untagged interactions, in which both interacting photons have $Q^2\approx 0$.

One of the spin-one resonances was observed at an invariant mass of 1273 ± 11 MeV/c^2 in the final state $\eta\pi^+\pi^-$ ($\eta\to\gamma\gamma$). Although low statistics and theoretical uncertainties did not permit a conclusive determination of its parity, all its properties were consistent with those of the $f_1(1285)$. We assumed in the remainder of the analysis that the signal was in fact due to the reaction $e^+e^-\to e^+e^-f_1(1285)$. To check the Monte Carlo calculation of our $\eta\pi^+\pi^-$ acceptance, we analyzed the $\eta'(958)$ signal seen in the same final state; our results, shown in Fig. 4, agreed with previous measurements of its formation by $\gamma\gamma$ fusion.

As discussed in Sec. II, the strength of the $\gamma\gamma$-$f_1(1285)$ coupling is expressed by a parameter $\tilde{\Gamma}_{\gamma\gamma}(f_1(1285))$; its Q^2 dependence (when one of the virtual photons is nearly real) is described by a function $\tilde{F}^2(Q^2)$, which vanishes as Q^2 approaches zero. The measured cross section for the reaction $e^+e^-\to e^+e^-f_1(1285)$ and the corresponding values of $\tilde{F}^2(Q^2)\tilde{\Gamma}_{\gamma\gamma}(f_1(1285))$ are shown in Fig. 5. We used the form of the function $\tilde{F}^2(Q^2)$ specified by the Cahn model[24] for the formation of $q\bar{q}$ mesons with $J^{PC}=1^{++}$ to determine the value of $\tilde{\Gamma}_{\gamma\gamma}(f_1(1285))$ (Refs. 28) that best fit our tagged $\eta\pi^+\pi^-$ data. Assuming that the unknown form factor $F(Q^2)$ in the Cahn model is given by $F_\rho(Q^2)=(1+Q^2/M_\rho^2)^{-1}$, we found $\tilde{\Gamma}_{\gamma\gamma}(f_1(1285))=2.4\pm 0.5\pm 0.5$ keV. Invariant-mass spectra obtained from analyses of the $\pi^+\pi^-\pi^+\pi^-$ and $K^\pm K_S^0\pi^\mp$ ($K_S^0\to\pi^+\pi^-$) final states were consistent with this value.

Our observation of a spin-one meson in the $K^\pm K_S^0\pi^\mp$ ($K_S^0\to\pi^+\pi^-$) final state was first reported in Ref. 1. We found in the analysis presented here that the mass, width, and decay distributions of this resonance, which we call the $X(1420)$, were consistent with those of the $f_1(1420)$, an isoscalar, spin-one state seen in hadronic interactions.[15,16] However, with our present statistics, we were unable to exclude the possibility that the $X(1420)$ is a $q\bar{q}g$ hybrid with the exotic quantum numbers $J^{PC}=1^{-+}$. The cross section for $e^+e^-\to e^+e^-X(1420)\to e^+e^-K\bar{K}\pi$ and the corresponding values of $B_{K\bar{K}\pi}\tilde{F}^2(Q^2)\tilde{\Gamma}_{\gamma\gamma}(X(1420))$ are shown in Fig. 10. With $\tilde{F}^2(Q^2)$ as specified by the Cahn model, our data were best fit by the value $B_{K\bar{K}\pi}\tilde{\Gamma}_{\gamma\gamma}(X(1420))=0.63\pm 0.24\pm 0.15$ keV assuming $F=F_\phi$, or $1.3\pm 0.5\pm 0.3$ keV assuming $F=F_\rho$. As this difference illustrates, $\tilde{\Gamma}_{\gamma\gamma}$ values extracted from our data are extremely sensitive to the choice of a particular model. There is, on the other hand, very little model dependence in the results shown in Figs. 5 and 10.

If the $X(1420)$ is a member of the axial-vector-meson nonet containing the $f_1(1285)$, then the ratio of its $\gamma\gamma$ coupling parameter to that of the $f_1(1285)$ is related to θ_A, the singlet-octet mixing angle of that nonet. To extract θ_A we assumed that $B_{K\bar{K}\pi}\approx 1$, and that the radial wave functions of the SU(3)-singlet and -octet states have equal derivatives at the origin. Using the values for $\tilde{\Gamma}_{\gamma\gamma}(f_1(1285))$ and $B_{K\bar{K}\pi}\tilde{\Gamma}_{\gamma\gamma}(X(1420))$ derived assuming a ρ form factor and a ϕ form factor, respectively, we found $\theta_A=(45.4\pm 6.2)°$. This value is in excellent agreement with the 42.2° predicted by the Gell-Mann–Okubo quadratic mass formula, less so with the ideal mixing angle, $\theta_I\approx 35.3°$. The $X(1420)$ is thus unlikely to be a pure $s\bar{s}$ state belonging to the same meson nonet as the $f_1(1285)$, if all our assumptions are valid. If the $X(1420)$ is a member of the axial-vector-meson nonet, then our result would imply that its quark content is a mixture of about 3% $(u\bar{u}+d\bar{d})/\sqrt{2}$ with 97% $s\bar{s}$. Using a ρ form factor to determine $\tilde{\Gamma}_{\gamma\gamma}(X(1420))$, or assuming $B_{K\bar{K}\pi}<1$,

leads to mixing angles farther from θ_I, and hence to greater light-quark content for the $X(1420)$.

It has been proposed that the $f_1(1530)$, rather than the $X(1420)$, is the f_1', and that the $X(1420)$ is an exotic state of composition $q^2\bar{q}^2$ (Ref. 21) or $q\bar{q}g$ (Ref. 22). At present, we are unable to draw any conclusions regarding the correctness of these proposals. If more specific predictions regarding the formation of these exotic states become available, higher-statistics $\gamma\gamma$ fusion data may play a useful part in determining whether the $X(1420)$ is the f_1', and, if not, in distinguishing among the other possibilities.

ACKNOWLEDGMENTS

We wish to acknowledge useful discussions with Robert Cahn. We thank the PEP staff for their dedication and productive running of the machine, and our engineers and technicians for their efforts in the construction and maintenance of the detector. This work was supported in part by the United States Department of Energy, the National Science Foundation, the Joint Japan–United States Collaboration in High Energy Physics, and the Foundation for Fundamental Research on Matter in the Netherlands.

[1]TPC/Two-Gamma Collaboration, H. Aihara *et al.*, Phys. Rev. Lett. **57**, 2500 (1986).

[2]Mark II Collaboration, G. Gidal *et al.*, Phys. Rev. Lett. **59**, 2016 (1987).

[3]JADE Collaboration, W. Bartel *et al.*, contribution to the 1987 International Europhysics Conference on High-Energy Physics, Uppsala, Sweden, 1987 (unpublished).

[4]Mark II Collaboration, G. Gidal, *et al.*, Phys. Rev. Lett. **59**, 2012 (1987).

[5]L. F. Landau, Dok. Akad. Nauk USSR **60**, 207 (1948).

[6]C. N. Yang, Phys. Rev. **77**, 242 (1950).

[7]J. L. Rosner, Phys. Rev. D **27**, 1101 (1983).

[8]H. Kolanoski, *Two-Photon Physics at e^+e^- Storage Rings* (Springer Tracts in Modern Physics, Vol. 105) (Springer, Berlin, 1984).

[9]M. Poppe, Int. J. Mod. Phys. **1**, 545 (1986).

[10]Ch. Berger and W. Wagner, Phys. Rep. **146**, 1 (1987).

[11]Particle Data Group, M. Aguilar-Benitez *et al.*, Phys. Lett. **170B**, 1 (1986). We employ the new meson nomenclature, described in this reference. Some of the new names are $\eta(1440)$, formerly ι, $f_1(1420)$, formerly E, $f_1(1285)$, formerly D, and $a_0(980)$, formerly δ.

[12]S. I. Bityukov *et al.*, Phys. Lett. B **203**, 327 (1988).

[13]Mark III Collaboration, J. J. Becker *et al.*, Phys. Rev. Lett. **59**, 186 (1987); Mark III Collaboration, L. Köpke *et al.*, in *Proceedings of the XXIII International Conference on High-Energy Physics*, Berkeley, California edited by S. C. Loken (World Scientific, Singapore, 1987), p. 692.

[14]DM2 Collaboration, B. Jean-Marie *et al.*, in *Proceedings of the XXIII International Conference on High-Energy Physics* (Ref. 13), p. 652.

[15]C. Dionisi *et al.*, Nucl. Phys. **B169**, 1 (1980).

[16]T. A. Armstrong *et al.*, Phys. Lett. **146B**, 273 (1984).

[17]LASS Collaboration, D. Aston *et al.*, Phys. Lett. B **201**, 573 (1988).

[18]The state observed recoiling against an $\omega(783)$ or $\phi(1020)$ had a mass of $1442\pm7^{+10}_{-20}$ MeV/c^2, and a width of $40^{+17}_{-13}\pm10$ MeV. It is stated in Ref. 13 that the measured width is inconsistent (at the 90% confidence level) with that of the $\eta(1440)$.

[19]A Seiden, H. F. W. Sadrozinski, and H. E. Haber, University of California, Santa Cruz, Institute for Particle Physics Report No. SCIPP-87-73, 1987 (unpublished).

[20]Ph. Gavillet *et al.*, Z. Phys. C **16**, 119 (1982).

[21]D. O. Caldwell, Mod. Phys. Lett. **A2**, 771 (1987).

[22]M. Chanowitz, Phys. Lett. B **187**, 409 (1987).

[23]M. Zielinski, Phys. Rev. Lett. **58**, 2002 (1987).

[24]Robert N. Cahn, Phys. Rev. D **35**, 3342 (1987); **37**, 833 (1988).

[25]V. M. Budnev, I. F. Ginzburg, G. V. Meledin, and V. G. Serbo, Phys. Rep. **15C**, 181 (1975).

[26]The ratio $W^2/2\sqrt{X}$ is unity when both Q_1^2 and Q_2^2 are zero. Hence the power to which this ratio appears in Eq. (3) represents a choice of convention that affects the functions $\Gamma_{\gamma^*\gamma^*}(Q_1^2,Q_2^2,W^2)$ defined here, but not its limit as both Q^2 values approach zero. Our choice is in accord with the convention of Ref. 9.

[27]G. Köpp, T. F. Walsh, and P. Zerwas, Nucl. Phys. **B70**, 461 (1974). Note that our normalization of the $\gamma\gamma^*$ form factor differs from that used in this reference.

[28]Cahn's definition of $\Gamma^{IJ}_{\gamma^*\gamma^*}(Q_1^2,Q_2^2,W^2)$ for $J\neq1$ leads, for a given cross section, to $\Gamma^{IJ}_{\gamma^*\gamma^*}$ and $\Gamma^{IJ}_{\gamma\gamma^*}$ functions greater by a factor $2\sqrt{X}/W^2$ than those defined by Eqs. (3) and (4); in the case of $\Gamma^{IJ}_{\gamma\gamma^*}(Q^2,W^2)$, this factor is equal to $1+Q^2/W^2$. When $J=1$, Cahn's functions are greater than ours by the factor $4\sqrt{X}/W^2$; in the case of $\Gamma_{\gamma\gamma^*}(Q^2,W^2)$, this factor approaches 2 as Q^2 approaches zero. The definition in Eq. (7) consequently results in his $\tilde{\Gamma}_{\gamma\gamma}$ values being greater than ours by a factor of 2. More specifically, his $J=1$ analog of Eq. (3) would have the constant 16π, rather than our 32π. The 32π includes a factor of 2 related to the identity of the two photons, which is needed if Eq. (5) is to be true for $J\neq1$. In the $J=1$ case, Eq. (5) is true trivially with either convention, but we prefer to use the same constant in Eq. (3) for all spins. Our preference is motivated by the fact that, regardless of the spin of the resonance formed, the two virtual photons participating in a $\gamma\gamma$ fusion reaction are never "identical" (i.e., their Q^2 values differ except in a phase-space subset of measure zero). There is thus no good reason to treat Eq. (3) differently in the spin-one case. We emphasize that the physical cross section for the reaction $e^+e^-\to e^+e^-A$ does not depend on the convention chosen.

[29]J. Olsson, Report No. DESY-87-136, 1987 (unpublished). See pp. 14 and 15, and particularly Fig. 28.

[30]More precisely, ϵ^{-1} is the average value of $\mathcal{L}_{TT}/\mathcal{L}_{LT}$ for events with a positron tag, and the average value of $\mathcal{L}_{TT}/\mathcal{L}_{TL}$ for events with an electron tag.

[31]TPC/Two-Gamma Collaboration, H. Aihara *et al.*, Lawrence Berkeley Laboratory Report No. LBL-23737 (unpublished).

[32]Marjorie D. Shapiro, Ph.D. thesis, Lawrence Berkeley Laboratory Report No. LBL-18820, 1984.

[33]See, for example, TPC/Two-Gamma Collaboration, H. Aihara *et al.*, Phys. Rev. Lett. **57**, 404 (1986).

[34]Events with low-energy photon conversions are not likely to be a significant source of background, since the energy and point of origin of TPC e^+e^- pairs were relatively well measured; converted photons were therefore exempt from the 125-MeV photon energy cuts made after the 2C and 3C fits described in Sec. IV.

[35]Mark II Collaboration, G. S. Abrams *et al.*, Phys. Rev. Lett. **43**, 477 (1979); Mark II Collaboration, P. Jenni *et al.*, Phys. Rev. D **27**, 1031 (1983).

[36]JADE Collaboration, W. Bartel *et al.*, Phys. Lett. **113B**, 190 (1982).

[37]CELLO Collaboration, H. J. Behrend *et al.*, Phys. Lett. **114B**, 378 (1982); **125B**, 518(E) (1983).

[38]PLUTO Collaboration, Ch. Berger, *et al.*, Phys. Lett. **142B**, 125 (1984).

[39]TASSO Collaboration, M. Althoff *et al.*, Phys. Lett. **147B**, 487 (1984).

[40]TPC/Two-Gamma Collaboration, H. Aihara *et al.*, Phys. Rev. D **35**, 2650 (1987).

[41]Crystal Ball Collaboration, D. Antreasyan *et al.*, Phys. Rev. D **36**, 2633 (1987).

[42]H. Albrecht *et al.*, Phys. Lett. B **199**, 457 (1987).

[43]J. J. Sakurai, Ann. Phys. (N.Y.) **11**, 1 (1960); Phys. Rev. Lett. **22**, 981 (1969).

[44]N. Stanton *et al.*, Phys. Rev. Lett. **42**, 346 (1979).

[45]A. Ando *et al.*, Phys. Rev. Lett. **57**, 1296 (1986).

[46]A. Kolmogorov, Inst. Ital. Attuari Giorn. **4**, 1 (1933); A. G. Frodesen, O. Skjeggestad, and H. Tøfte, *Probability and Statistics in Particle Physics* (Universitetsforlayet, Bergen, 1979), p. 424.

[47]W. Feller, Ann. Math. Stat. **19**, 177 (1948).

[48]H. Grässler *et al.*, Nucl. Phys. **B121**, 189 (1977).

[49]M. J. Corden *et al.*, Nucl. Phys. **B144**, 253 (1978).

[50]A. Gurtu *et al.*, Nucl. Phys. **B151**, 181 (1979).

[51]A Monte Carlo simulation of $f_1(1285)$ formation using a three-body phase-space decay, but modified so that the distribution of $\cos\theta^*$ was still given by $1+\cos^2\theta^*+2\mathcal{R}_{\rm Cahn}\sin^2\theta^*$, resulted in an average acceptance approximately 8% less than the result obtained using an $a_0(980)\pi$ decay.

[52]We have divided the $\tilde{\Gamma}_{\gamma\gamma}$ values reported in Refs. 2 and 4 by 2, to convert them to the convention defined by Eqs. (3) and (7); see also Ref. 28.

[53]Reference 4 presents values for $\tilde{\Gamma}_{\gamma\gamma}(f_1(1285))$ derived from data in two Q^2 bins. In order to convert these results to the quantity shown in Fig. 5(b), and to our conventions (as defined in Sec. II), we have multiplied each value given in Ref. 4 by $\tilde{F}_\rho^2(Q^2)/2$. In this expression, $\tilde{F}_\rho(Q^2)$ is the spin-one effective form factor predicted by the Cahn model with $F=F_\rho$, evaluated at the location in Q^2 of each point shown in Ref. 4.

[54]The effect of scaling the pion momenta is quite small: if δM is the difference between the $K^\pm K_S^0\pi^\mp$ invariant masses calculated using scaled and unscaled pion momenta, then $\langle(\delta M)\rangle\approx 0$ and $[\langle(\delta M)^2\rangle]^{1/2}\approx 12$ MeV/c^2.

[55]By $K^*(892)K$ we mean here an equal mixture of $K^{*0}(892)\bar{K}^0$, $\bar{K}^{*0}(892)K^0$, $K^{*+}(896)K^-$, and $K^{*-}(896)K^+$.

[56]F. M. Renard, Nuovo Cimento **80A**, 1 (1984).

[57]Sadao Oneda and Akihito Miyazaki, Kyoto University Research Institute for Fundamental Physics Report No. RIFP-710, 1987 (unpublished).

[58]There is some theoretical ambiguity regarding the power to which the ratio of the masses should appear. The equation used by the Mark II Collaboration does not contain this ratio.

[59]D. Morgan and M. R. Pennington, Z. Phys. C **37**, 441 (1988). The authors warn that some of the assumptions used to extract $\Gamma_{\gamma\gamma}(f_2(1270))$ from $\gamma^*\gamma^*-<\pi^+\pi^-$ data may not be justified.

[60]The quoted uncertainties were derived by assuming that the distributions of many measurements of the numerator and denominator of this ratio would be described by Gaussians whose standard deviations are equal to the combination in quadrature of the statistical and systematic uncertainties given in Secs. VI and IX for the numerator and denominator, respectively. The central value of the ratio is defined to be the median value of the resulting distribution of ratios. The uncertainties, added to the central value, yield the values of the ratio such that 34% of the entries in the predicted distribution of the ratios lie between each of these values and the median.

[61]The Mark II Collaboration's measured ratio $\tilde{\Gamma}_{\gamma\gamma}(f_1(1285))/\tilde{\Gamma}_{\gamma\gamma}(X(1420))$, given in Ref. 4, is 3.0 ± 1.8. If used in Eq. (22), this value would imply $\theta_A=(48.2^{+12.2}_{-5.3})^\circ$ and $\lambda=(-13.0^{+5.3}_{-12.2})^\circ$.